Received 21 September 2022; revised 4 November 2022; accepted 19 November 2022. Date of publication 25 November 2022; date of current version 19 December 2022.

Digital Object Identifier 10.1109/OJCOMS.2022.3224835

Second Order Statistics of *N*-Fisher-Snedecor $\mathcal{F}$ Distribution and Their Application to Burst Error Rate Analysis of Multi-Hop Communications

CASLAV M. STEFANOVIC [1] (Member, IEEE), ANA GARCÍA ARMADA [1] (Senior Member, IEEE), AND XAVIER COSTA-PÉREZ [2,3,4] (Senior Member, IEEE)

[1]Department of Signal Theory and Communications, Universidad Carlos III de Madrid, 28911 Leganés, Spain

[2]i2CAT Foundation, 08034 Barcelona, Spain

[3]ICREA, 08010 Barcelona, Spain

[4]6G, NEC Laboratories Europe, 08034 Barcelona, Spain

CORRESPONDING AUTHOR: C. M. STEFANOVIC (e-mail: cstefano@ing.uc3m.es)

This work was supported in part by UC3M and the European Union's Horizon 2020 Programme under the Marie Skłodowska-Curie Grant through the CONEX-Plus Project under Agreement 801538; in part by the IRENE-EARTH Project under Grant PID2020-115323RB-C33/AEI/10.13039/501100011033; in part by ERDF and the Spanish Government Projects under Grant PID2019-106808RA-I00 AEI/FEDER, UE; in part by CDTI Cervera Project INTEGRA under Grant CER-20211031; in part by the Secretaria d'Universitats i Recerca de la Generalitat de Catalunya under Project 2017-SGR-00376 and Project Fem IoT under Grant 001-P-001662; in part by the European Commission Project CPSoSaware; and in part by the Cost Actions under Grant CA19111, Grant CA20120, and Grant CA16220.

ABSTRACT An advantage of using the composite fading models (CFMs) is their ability to concurrently address the impact of multi-path and shadowing phenomena on the system performance in wireless communications. A Fisher-Snedecor (FS) $\mathcal{F}$ CFM has been recently proposed as an experimentally verified and tractable fading model that can be efficiently applied for 5G and beyond 5G wireless communication systems. This paper provides second-order (s-order) performance analysis of the product of N independent but not identically distributed (i.n.i.d) FS $\mathcal{F}$ random variables (RVs). In particular, accurate and closed-form approximations for level crossing rate (LCR) and average fade duration (AFD) of the product of N i.n.i.d FS $\mathcal{F}$ (N-FS $\mathcal{F}$) RVs are successfully derived by exploiting a general property of a Laplace approximation method for evaluation of the N-folded integral-form LCR expression. Based on the obtained s-order statistical results, the burst error rate and maximum symbol rate of the N-FS $\mathcal{F}$ distribution are addressed and thoroughly examined. The numerical results of the considered performance measures are discussed in relation to the N-FS $\mathcal{F}$ multi-path and shadowing severity parameters. Moreover, the impact of the number of hops (N) of the N-FS $\mathcal{F}$ CFM on the s-order metrics, the burst error rate and maximum symbol rate are numerically evaluated and investigated. The derived s-order statistical results can be used to address the cooperative relay-assisted (RA) communications for vehicular systems. Monte-Carlo (M-C) simulations for the addressed statistical measures are developed in order to confirm the provided theoretical results.

INDEX TERMS 5G, 6G, burst error rate, composite fading model (CFM), Fisher-Snedecor (FS) $\mathcal{F}$ distribution, second-order (s-order) statistics, vehicular communications.

I. INTRODUCTION

WIRELESS communications are one of the key technologies that shape our everyday life. The emergence of wirelessly connected nodes for 5G and beyond not only include mobile phones, but also vehicles, trains, unmanned-aerial-vehicles (UAVs), machines and many other connected devices. Channel characterization and performance analysis of such devices become an essential task for designing and deploying inter-connected wireless systems.

Wireless communications are highly affected by the propagation environment mainly due to multi-path fading and shadowing phenomena [1]. The importance of the composite

fading models (CFMs) is crucial due to their property to incorporate the simultaneous effect of the multi-path and shadowing on the system performances. The CFMs that are based on the mixture of log-normal random variables (RVs) have been reported in [2], [3]. Although the log-normal RVs are in accordance with the experiments for the shadowing effect, the performance analysis and mathematical manipulations with log-normal RVs can often lead to complex analytical expressions. In [4], [5], authors considered a Gamma-shadowed Nakagami-m distribution and provided theoretical verification for the Gamma RV as an adequate substitute for the log-normal RV. The communication systems over K and general-K composite fading channels have been addressed in [6] and [7], respectively. Moreover, the CFMs that can be applied in a variety of propagation scenarios are based on the mixture of some general and Gamma distributions [8], [9], [10].

The recently proposed composite Fisher-Snedecor (FS) $\mathcal{F}$ fading distribution is modeled with Nakagami-m and inverse Nakagami-m (I-Nakagami-m) RVs, where the average power of a Nakagami-m RV is subjected to the variations caused by an I-Nakagami-m RV [11]. It is important to note that the Nakagami-m distribution is capable of approximating the Rician distribution [12], which makes the FS $\mathcal{F}$ CFM attractive for application in line-of-sight (LOS) as well as non-LOS (N-LOS) multi-path/shadowing environments. The FS $\mathcal{F}$ CFM is confirmed by experiments for wireless communication between two nodes and has turned out to be mathematically more tractable than other CFMs. Moreover, FS $\mathcal{F}$ CFM has been efficiently applied for channel modeling and performance evaluation of re-configurable intelligent surface (RIS) assisted communications [13], [14], [15], [16], [17]. In [18], simultaneous wireless information and power transfer (SWIPT) networks in the presence of FS $\mathcal{F}$ fading are addressed. The diversity reception with selection-combining (SC) and switched-and-stayed-combining (SSC) over the FS $\mathcal{F}$ fading channel have been explored in [19] and [20], respectively. Furthermore, statistics of the sum of FS $\mathcal{F}$ RVs with application to maximal-ratio-combining (MRC) are addressed in [21], [22]. Performance evaluation of dual-hop amplify-and-forward (AF) relay-assisted (RA) communications over the FS $\mathcal{F}$ fading channels is considered in [23]. Considerable efforts have been made in performance analysis of the channel capacity over FS $\mathcal{F}$ composite fading channels. In particular, a comprehensive study of the achievable channel capacity in the presence of FS $\mathcal{F}$ channels under different channel-state-information (CSI) availability assumptions has been explored in [24]. The ergodic channel capacity over the FS $\mathcal{F}$ fading under different power adaptation schemes are thoroughly addressed in [25], [26]. Furthermore, the effective channel capacity as well as the effective channel capacity in high SNR regime for single-input single-output (SISO) and multiple-input single-output (MISO) configurations are investigated in [27], [28]. Effective rate and achievable fixed rate capacity over composite $\mathcal{F}$ fading channels for emerging wireless systems such as vehicular communications are provided in [29], [30]. Physical layer security (PLS) over FS $\mathcal{F}$ fading channels are addressed in [31], [32]. Furthermore, the performance evaluation of wireless multiple access communication links over correlated FS $\mathcal{F}$ fading is investigated in [33]. The energy detection based spectrum sensing by applying FS $\mathcal{F}$ CFM is considered in [34]. In [35], authors introduced cascaded N-Fisher-Snedecor (N-FS) $\mathcal{F}$ distribution modeled as the product of N independent but not identically distributed (i.n.i.d) RVs and provided statistics such as probability density function (PDF), cumulative distribution function (CDF) and moment generating function (MGF). Capitalizing on the obtained results, [35] provided further outage probability and bit error rate as the important system performance measures of the cascaded N-FS $\mathcal{F}$ CFM. Moreover, the performance analysis of products and ratio of the products of FS $\mathcal{F}$ RVs and their applications to wireless communication scenarios are investigated in [36], [37]. Indeed, the products and the ratios of RVs play a significant role in wireless communications, since the products can be used to assess the performance of multi-hop relaying, keyhole MIMO communications, RIS assisted communications, RFID systems and multiple-scattered, multiple-shadowed fading environments [35], [36], [38], [39], [40], [41], [42], [43], while the ratio of RVs can be used in interference limited environments, spectrum sharing or full duplex communications [36], [37], [44], [45], [46].

However, the references mentioned above are only limited to the first-order (f-order) statistical performances of the various fading models. In order to get a better insight into the behaviour of time-variant channels, second-order (s-order) statistical analysis is important. The level crossing rate (LCR) and average fade duration (AFD) are widely considered as s-order statistical measures since they can be addressed through the integration of the first derivative of N-FS $\mathcal{F}$ random process (RP) and take into account the movement of the communicating objects [12], [47]. In particular, the LCR of N-FS $\mathcal{F}$ distribution is the time rate of change of the composite faded signal, while the AFD of N-FS $\mathcal{F}$ distribution is the mean time of the composite faded signal's being below a specified threshold. The s-order performance analysis can be practically used for optimal interleaver and channel coding design of wireless systems over fading channels. Furthermore, the s-order statistics and Doppler characterization provide useful knowledge of time-variant composite fading channels for a variety of 5G and beyond 5G scenarios [48], [49], [50], [51].

The s-order statistics of the composite $\mathcal{F}$ distribution are considered in [52] whereas the s-order statistics of a bivariate FS $\mathcal{F}$ CFM are considered in [53]. Furthermore, the LCR and AFD of FS $\mathcal{F}$ turbulence induced fading channels for N-hop free-space-optical (FSO) communications and dual-hop RIS assisted FSO communications are investigated in [54], [55], respectively. The s-order statistics of CFM has been reported in [56]. Additionally, the s-order metrics of cascaded and multi-hop communications have been

extensively addressed in [57], [58], [59], [60], [61], [62] while s-order statistics of cooperative multi-hop communications with parallel links are addressed in [63], [64]. Namely, the available s-order statistical results of the N-hop cascaded fading channels for radio-frequency (RF) communications are only limited to N-Rayleigh and N-Nakagami-m channel models [57], [58], [59], [60], [61], [62], [65]. However, to the best of the authors' knowledge there is no reported results on the s-order statistics of the composite N-hop cascaded radio-frequency (RF) fading channels.

This paper provides the mathematical framework for calculation of novel, accurate and fast-to-compute closed-form s-order statistical measures such as LCR and AFD of N-FS $\mathcal{F}$ RF CFM. The general Laplace approximation (GLA) method has been exploited for derivation of closed-form approximations for LCR and AFD. The derived s-order statistics for the observed set of identically and non-identically distributed fading parameters are confirmed by Monte-Carlo (M-C) simulations. Moreover, capitalizing on the derived s-order statistical results and motivated by the fact that the available results for the burst error rate of cascaded fading channels are only limited to the dual-hop Nakagami-m and N-Nakagami-m fading channels [61], [66], we provide the burst error rate and maximum symbol rate for multi-hop communications over composite N-FS $\mathcal{F}$ fading channels which are based on the experimentally verified FS $\mathcal{F}$ CFM [11]. One need to have in mind that the N-FS $\mathcal{F}$ CFM can be used to capture propagation conditions more realistically if compared to N-Nakagami-m [61], since N-FS $\mathcal{F}$ CFM takes into account the simultaneous effect of the multi-path and shadowing on the multi-hop communication system. In the numerical results, novel remarks on the impact of N, multi-path and shadowing severity values of N-FS $\mathcal{F}$ CFM on the s-order measures, the burst error rate and maximum symbol rate have been drawn, graphically presented and analyzed in detail. Furthermore, the obtained s-order statistical measures of N-FS $\mathcal{F}$ distribution are compared to the previously published s-order statistical results for the special case when $N = 1$. Lastly, the obtained s-order results of N-FS $\mathcal{F}$ CFM are directly applied to cooperative communications established through independent direct link and independent multi-hop AF-RA links with selection-strategy (S-S) at reception.

The main contributions of this work are listed below:

- Derivation of novel closed-form mathematical expressions for PDF and CDF of double FS $\mathcal{F}$ distribution, modeled as the product of two i.n.i.d FS $\mathcal{F}$ RVs and expressed in terms of hypergeometric functions.
- Derivation of novel integral-form mathematical expressions for LCR and AFD of N-FS $\mathcal{F}$ distribution, modeled as the product of N i.n.i.d FS $\mathcal{F}$ RVs.
- Derivation of the closed-form approximations for LCR and AFD of N-FS $\mathcal{F}$ distribution using the general Laplace approximation (GLA) formula and validation of the obtained closed-form formulas through simulations.
- Performance analysis of the burst error rate and maximum symbol rate of AF-RA multi-hop communications over FS $\mathcal{F}$ fading channels based on the s-order statistics.
- S-order and burst error rate performance analysis of cooperative communications established through direct link and AF-RA multi-hop links over FS $\mathcal{F}$ channels with S-S at reception.
- Analysis of the impact of N-FS $\mathcal{F}$ CFM system model parameters on the s-order statistics and burst error rate of the multi-hop and cooperative multi-hop AF-RA communications where the novel remarks have been provided.

In particular, the obtained s-order statistical results can be useful in designing cooperative vehicular systems established through independent direct, multi-hop and cooperative multi-hop AF-RA links under LOS, N-LOS and N-LOS vehicle (N-LOSv) conditions with S-S at the destination. Indeed, vehicle-to-everything (V2X) 5G New Radio (NR) release 16 introduces the stochastic model for channel characterization in V2X communications where a path-loss formula is dependent on LOS, N-LOS and N-LOSv conditions [67]. The N-LOSv communication conditions are introduced to address the presence of blocking vehicles in V2X communications. Thus, the AF-RA vehicle-to-vehicle (V2V) communications can be used in vehicular networks in the absence of LOS V2V conditions [68], [69], [70], [71]. Moreover, the selection and switching strategies can be efficiently deployed in vehicular systems [49], [72], [73], [74], [75].

The paper is structured as follows. Sections II and III introduce FS $\mathcal{F}$ and double FS $\mathcal{F}$ CFMs, respectively. The s-order system performance analysis of N-FS $\mathcal{F}$ CFM modeled as the product of N i.n.i.d FS $\mathcal{F}$ RVs is presented in Section IV. In Section V, the s-order system performance analysis of multi-hop and cooperative multi-hop communications is considered. The numerical results and simulation results are given in Section VI. Lastly, Section VII concludes this paper.

The abbreviations that are used throughout the text are summarized in alphabetical order in Table 1.

II. FISHER-SNEDECOR $\mathcal{F}$ COMPOSITE FADING MODEL

The recently proposed Fisher-Snedecor (FS) $\mathcal{F}$ composite fading distribution is modeled with independent but not identically distributed (i.n.i.d) Nakagami-m and I-Nakagami-m RVs, where the average power of a Nakagami-m RV is subjected to the variations caused by an I-Nakagami-m RV [11]. The FS $\mathcal{F}$ RP, $Z_{\mathcal{F}}(t)$ can be expressed as

$$Z_{\mathcal{F}}(t) = X_{nm}(t)Y_{Inm}(t) = X_{nm}(t)\frac{1}{Y_{nm}(t)} \tag{1}$$

where $X_{nm}(t)$ and $Y_{Inm}(t)$ are Nakagami-m and I-Nakagami-m RPs, respectively (where the time t is omitted in the following text for simpler notation). Since the I-Nakagami-m RV can be expressed as $Y_{Inm} = \frac{1}{Y_{nm}}$, the

TABLE 1. Abbreviations used throughout the text.

Abbreviation	Definition
5G	5th Generation
6G	6th Generation
AF-RA	Amplify-and-forward relay-assisted
AFD	Average fade duration
CDF	Cumulative distribution function
CFM	Composite fading model
D2D	Device-to-device
f-order	First-order
FG	Fixed-gain
FSO	Free-space-optical
GLA	General Laplace approximation
i.n.i.d	Independent but not identically distributed
I-Nakagami-m	Inverse Nakagami-m
LCR	Level crossing rate
LOS	Line-of-sight
M-C	Monte Carlo
MGF	Moment generating function
MIMO	Multiple-input multiple-output
MISO	Multiple-input single-output
MRC	Maximal-ratio-combining
N-FS $\mathcal{F}$	N-Fisher-Snedecor $\mathcal{F}$
N-LOS	Non line-of-sight
N-LOSv	Non line-of-sight vehicle
NR	New Radio
PDF	Probability density function
PLS	Physical layer security
RF	Radio-frequency
RFID	Radio-frequency identification
RIS	Re-configurable intelligent surface
RP	Random process
RV	Random variable
s-order	Second-order
SC	Selection-combining
S-S	selection-strategy
SISO	Single-input single-output
SNR	Signal-to-noise ratio
SSC	Switch-and-stay-combining
SWIPT	Simultaneous wireless information and power transfer
UAV	Unmanned aerial vehicle
V2X	Vehicle-to-everything
ZM	Zero-mean

PDF of X_{nm} and Y_{nm} are [47, eq. (2.52)], respectively

$$p_{X_{nm}}(x_{nm}) = \frac{2(m_m/\Omega_m)^{m_m}}{\Gamma(m_m)} x_{nm}^{2m_m-1} e^{-\frac{m_m}{\Omega_m}x_{nm}^2} \quad (2)$$

$$p_{Y_{nm}}(y_{nm}) = \frac{2((m_s-1)/\Omega_s)^{m_s}}{\Gamma(m_s)} y_{nm}^{2m_s-1} e^{-\frac{(m_s-1)}{\Omega_s}y_{nm}^2} \quad (3)$$

where $\Gamma(\cdot)$ is the Gamma function [76, (eq. (8.310.1)]. The multi-path and shadowing severity parameters are m_m and m_s, respectively whereas the average powers of Nakagami-m and I-Nakagami-m RVs are Ω_m and Ω_s, respectively. The PDF of $Z_{\mathcal{F}} = \frac{X_{nm}}{Y_{nm}}$ is [45, eq. (25)]

$$p_{Z_{\mathcal{F}}}(z_{\mathcal{F}}) = \int_0^\infty y_{nm} p_{X_{nm}}(z_{\mathcal{F}} \times y_{nm}) p_{Y_{nm}}(y_{nm}) dy_{nm} \quad (4)$$

From (2-4), and using [76, eq. (3.326.2)] and [76, eq. (8.384.1)], respectively, the PDF of $Z_{\mathcal{F}}$ can be written as

$$p_{Z_{\mathcal{F}}}(z_{\mathcal{F}}) = \frac{2\left(\frac{m_m}{\Omega_m}\right)^{m_m}\left(\frac{m_s-1}{\Omega_s}\right)^{m_s}(\Omega_s\Omega_m)^{m_m+m_s} z_{\mathcal{F}}^{2m_m-1}}{B(m_m,m_s)\left(\Omega_s m_m z_{\mathcal{F}}^2 + \Omega_m(m_s-1)\right)^{m_m+m_s}} \quad (5)$$

where $B(\cdot,\cdot)$ is the Beta function [76, eq. (8.380.1)]. It can be noticed that $p_{Z_{\mathcal{F}}}(z_{\mathcal{F}})$ in (5) for $\Omega_s = 1$ and $\Omega_m = \Omega$ reduces to the PDF of FS $\mathcal{F}$ distribution given by [35, eq. (3)]. The closed-form CDF of $Z_{\mathcal{F}}$ can be obtained from (5) by applying $F_{Z_{\mathcal{F}}}(z_{\mathcal{F}}) = \int_0^{z_{\mathcal{F}}} p_{Z_{\mathcal{F}}}(z_{\mathcal{F}}) dz_{\mathcal{F}}$ and [76, eq. (3.194.1)], respectively as

$$F_{Z_{\mathcal{F}}}(z_{\mathcal{F}}) = \frac{(m_m)^{m_m-1}\left(\frac{\Omega_s}{\Omega_m}\right)^{m_m} z_{\mathcal{F}}^{2m_m}}{\beta(m_m,m_s)(m_s-1)^{m_m}} \times {}_2F_1\left(m_m+m_s, m_m, m_m+1; -\frac{m_m\Omega_s z_{\mathcal{F}}^2}{(m_s-1)\Omega_m}\right) \quad (6)$$

where ${}_2F_1(\cdot,\cdot;\cdot;\cdot)$ is a hypergeometric function [76, eq. (9.100)]. Similarly, the $F_{Z_{\mathcal{F}}}(z_{\mathcal{F}})$ in (6) for $\Omega_m = \Omega$ and $\Omega_s = 1$, reduces to the CDF of FS $\mathcal{F}$ distribution. Moreover, the composite FS $\mathcal{F}$ CFM reduces to the fading models without shadowing such as Nakagami-m (for $m_s \to \infty$) and Rayleigh (for $m_s \to \infty$ and $m_m = 1$).

III. DOUBLE FISHER-SNEDECOR $\mathcal{F}$ COMPOSITE FADING MODEL

The product of two i.n.i.d FS $\mathcal{F}$ RPs can be written as

$$Z_{\mathcal{F}_d} = Z_{\mathcal{F}_1} Z_{\mathcal{F}_2} = X_{nm,1} Y_{Inm,1} X_{nm,2} Y_{Inm,2} = \frac{X_{nm,1}}{Y_{nm,1}} \frac{X_{nm,2}}{Y_{nm,2}} \quad (7)$$

The PDFs of $X_{nm,i}$ and $Y_{nm,i} = \frac{1}{Y_{Inm,i}}$, $i = 1, 2$ are, respectively

$$p_{X_{nm,i}}(x_{nm,i}) = \frac{2\left(\frac{m_{m_i}}{\Omega_{m_i}}\right)^{m_{m_i}} x_{n,i}^{2m_{m_i}-1}}{\Gamma(m_{m_i})} e^{-\frac{m_{m_i}}{\Omega_{m_i}}x_{nm,i}^2} \quad (8)$$

$$p_{Y_{nm,i}}(y_{nm,i}) = \frac{2\left(\frac{m_{s_i}-1}{\Omega_{s_i}}\right)^{m_{s_i}} y_{nm,i}^{2m_{s_i}-1}}{\Gamma(m_{s_i})} e^{-\left(\frac{m_{s_i}-1}{\Omega_{s_i}}\right)y_{nm,i}^2} \quad (9)$$

where m_{m_i} and m_{s_i} are the multi-path and shadowing severity parameters of double FS $\mathcal{F}$ CFM, respectively, whereas $\Omega_{m_i} = \Omega_i$ and $\Omega_{s_i} = 1$. The PDF of a double FS $\mathcal{F}$ RV $Z_{\mathcal{F}_d} = Z_{\mathcal{F}_1} Z_{\mathcal{F}_2}$ can be obtained from

$$p_{Z_{\mathcal{F}_d}}(z_{\mathcal{F}_d}) = \int_0^\infty \left|\frac{dz_{\mathcal{F}_1}}{dz_{\mathcal{F}_d}}\right| p_{Z_{\mathcal{F}_1}}\left(\frac{z_{\mathcal{F}_d}}{z_{\mathcal{F}_2}}\right) p_{Z_{\mathcal{F}_2}}(z_{\mathcal{F}_2}) dz_{\mathcal{F}_2} \quad (10)$$

where $|\frac{dz_{\mathcal{F}_1}}{dz_{\mathcal{F}_d}}| = z_{\mathcal{F}_2}^{-1}$. After substituting (8) and (9) in (10) and using [76, eq. (3.259.3)], closed-form PDF expression of double FS $\mathcal{F}$ RV in terms of hypergeometric function is derived and presented at the bottom of the next page. Moreover, by transforming RVs, $\gamma_{\mathcal{F}_d} = {z_{\mathcal{F}_d}}^2$, PDF of the SNR is obtained and provided as (12), shown at the bottom of the next page, where $\bar{\gamma}_i = \Omega_i$ is the average SNR value of double FS $\mathcal{F}$ CFM. The CDF of double FS $\mathcal{F}$ distribution can be obtained from $F_{Z_{\mathcal{F}_d}}(z_{\mathcal{F}_d}) = \int_0^{z_{\mathcal{F}_d}} p_{Z_{\mathcal{F}_d}}(x) dx$. By using (8-10), the $F_{Z_{\mathcal{F}_d}}(z_{\mathcal{F}_d})$ can be written as

$$F_{Z_{\mathcal{F}_d}}(z_{\mathcal{F}_d}) = \frac{4{m_{m_1}}^{m_{m_1}}(m_{s_1}-1)^{m_{s_1}}}{B(m_{m_1},m_{s_1})B(m_{m_2},m_{s_2})}$$

$$\times\, {m_{m_2}}^{m_{m_2}} \left(m_{s_2}-1\right)^{m_{s_2}} {\Omega_1}^{m_{s_1}} {\Omega_2}^{m_{s_2}} \times \int_0^{\infty} dz_{\mathcal{F}_2} \frac{{z_{\mathcal{F}_2}}^{2m_{m_2}+2m_{s_1}-1}}{\left(m_{m_2} z_{\mathcal{F}_2}^2 + \left(m_{s_2}-1\right)\Omega_2\right)^{m_{m_2}+m_{s_2}}} \times \int_0^{z_{\mathcal{F}_d}} \frac{x^{2m_{m_1}-1} dx}{\left(m_{m_1} x^2 + z_{\mathcal{F}_2}^2 \left(m_{s_1}-1\right)\Omega_1\right)^{m_{m_1}+m_{s_1}}} \quad (13)$$

By applying the variable substitution, $k = m_{m_1}x^2 + z_{\mathcal{F}_2}^2(m_{s_1}-1)\Omega_1$ and then by applying the binomial formula [76, eq. (1.111)] and [76, eq. (3.259.3)], the $F_{Z_{\mathcal{F}_d}}(z_{\mathcal{F}_d})$ closed form expression is derived for the integer values of m_{m_1} and presented as (14) shown at the bottom of the page. Similarly, the closed-form SNR CDF expression $F_{\gamma_{\mathcal{F}_d}}(\gamma_{\mathcal{F}_d})$, where $\bar{\gamma}_i = \Omega_i$ is given as (15), shown at the bottom of the page. In [35], authors introduced N-FS $\mathcal{F}$ CFM and provided the PDF and CDF of N-FS $\mathcal{F}$ distribution in terms of the Meijer's G functions. Although the Meijer's G functions are usually applied for obtaining useful and important analytical expressions they need to satisfy specific conditions [76, eq. (9.301)]. We provide useful and novel PDF and CDF expressions of double FS $\mathcal{F}$ RV given in terms of hypergeometric functions, where CDF is valid for integer values of m_{m_1}. Moreover, a similar analytical approach for derivation of the PDF and CDF of FSO RIS assisted communications over FS $\mathcal{F}$ turbulence channels has been performed in [55].

IV. N-FISHER-SNEDECOR $\mathcal{F}$ COMPOSITE FADING MODEL

The faded signal at the destination of cascaded N-FS $\mathcal{F}$ CFM can be modeled as the product of N i.n.i.d RPs

$$Z_{\mathcal{F}_N} = \prod_{i=1}^{N} Z_{\mathcal{F}_i} = \prod_{i=1}^{N} X_{nm,i} Y_{Inm,i} = \prod_{i=1}^{N} \frac{X_{nm,i}}{Y_{nm,i}} \quad (16)$$

$$p_{Z_{\mathcal{F}_d}}(z_{\mathcal{F}_d}) = 2\left(\frac{m_{m_1} m_{m_2}}{\left(m_{s_1}-1\right)\left(m_{s_2}-1\right)\Omega_1\Omega_2}\right)^{m_{m_2}} \frac{B\left(m_{m_2}+m_{s_1}, m_{m_1}+m_{s_2}\right)}{B\left(m_{m_1}, m_{s_1}\right)B\left(m_{m_2}, m_{s_2}\right)} {z_{\mathcal{F}_d}}^{2m_{m_2}-1} \times {}_2F_1\left(m_{m_2}+m_{s_2}, m_{m_2}+m_{s_1}; m_{m_1}+m_{s_1}+m_{m_2}+m_{s_2}; 1-\frac{m_{m_1} m_{m_2} {z_{\mathcal{F}_d}}^2}{\left(m_{s_1}-1\right)\left(m_{s_2}-1\right)\Omega_1\Omega_2}\right) \quad (11)$$

$$p_{\gamma_{\mathcal{F}_d}}(\gamma_{\mathcal{F}_d}) = \left(\frac{m_{m_1} m_{m_2}}{\left(m_{s_1}-1\right)\left(m_{s_2}-1\right)\bar{\gamma}_1\bar{\gamma}_2}\right)^{m_{m_2}} \frac{B\left(m_{m_2}+m_{s_1}, m_{m_1}+m_{s_2}\right)}{B\left(m_{m_1}, m_{s_1}\right)B\left(m_{m_2}, m_{s_2}\right)} {\gamma_{\mathcal{F}_d}}^{m_{m_2}-1} \times {}_2F_1\left(m_{m_2}+m_{s_2}, m_{m_2}+m_{s_1}; m_{m_1}+m_{s_1}+m_{m_2}+m_{s_2}; 1-\frac{m_{m_1} m_{m_2} \gamma_{\mathcal{F}_d}}{\left(m_{s_1}-1\right)\left(m_{s_2}-1\right)\bar{\gamma}_1\bar{\gamma}_2}\right) \quad (12)$$

$$F_{Z_{\mathcal{F}_d}}(z_{\mathcal{F}_d}) = \frac{\left(m_{s_1}-1\right)^{m_{s_1}} {m_{m_2}}^{m_{m_2}} \left(m_{s_2}-1\right)^{m_{s_2}}}{B\left(m_{m_1}, m_{s_1}\right)B\left(m_{m_2}, m_{s_2}\right)} \sum_{k=0}^{m_{m_1}-1} \binom{m_{m_1}-1}{k} (-1)^k \frac{\left(m_{s_1}-1\right)^k}{m_{s_1}+k} \times \left(\frac{\left(\frac{1}{m_{m_2}}\right)^{m_{m_2}} B\left(m_{m_2}, m_{s_2}\right)}{\left(m_{s_1}-1\right)^{m_{s_1}+k}\left(m_{s_2}-1\right)^{m_{s_2}}} - \frac{\left(\frac{1}{m_{s_1}-1}\right)^{m_{m_2}+m_{s_1}+k} {m_{m_1}}^{m_{m_2}} {z_{\mathcal{F}_d}}^{2m_{m_2}} B\left(m_{m_2}+m_{s_1}+k, m_{s_2}\right)}{\left(m_{s_2}-1\right)^{m_{m_2}+m_{s_2}} \left(\Omega_1\Omega_2\right)^{m_{m_2}}}\right) \times {}_2F_1\left(m_{m_2}+m_{s_2}, m_{m_2}+m_{s_1}+k; m_{s_1}+m_{m_2}+m_{s_2}+k; 1-\frac{m_{m_1} m_{m_2} {z_{\mathcal{F}_d}}^2}{\left(m_{s_1}-1\right)\left(m_{s_2}-1\right)\Omega_1\Omega_2}\right) \quad (14)$$

$$F_{\gamma_{\mathcal{F}_d}}(\gamma_{\mathcal{F}_d}) = \frac{\left(m_{s_1}-1\right)^{m_{s_1}} {m_{m_2}}^{m_{m_2}} \left(m_{s_2}-1\right)^{m_{s_2}}}{B\left(m_{m_1}, m_{s_1}\right)B\left(m_{m_2}, m_{s_2}\right)} \sum_{k=0}^{m_{m_1}-1} \binom{m_{m_1}-1}{k} (-1)^k \frac{\left(m_{s_1}-1\right)^k}{m_{s_1}+k} \times \left(\frac{\left(\frac{1}{m_{m_2}}\right)^{m_{m_2}} B\left(m_{m_2}, m_{s_2}\right)}{\left(m_{s_1}-1\right)^{m_{s_1}+k}\left(m_{s_2}-1\right)^{m_{s_2}}} - \frac{\left(\frac{1}{m_{s_1}-1}\right)^{m_{m_2}+m_{s_1}+k} {m_{m_1}}^{m_{m_2}} {\gamma_{\mathcal{F}_d}}^{m_{m_2}} B\left(m_{m_2}+m_{s_1}+k, m_{s_2}\right)}{\left(m_{s_2}-1\right)^{m_{m_2}+m_{s_2}} \left(\bar{\gamma}_1\bar{\gamma}_2\right)^{m_{m_2}}}\right) \times {}_2F_1\left(m_{m_2}+m_{s_2}, m_{m_2}+m_{s_1}+k; m_{s_1}+m_{m_2}+m_{s_2}+k; 1-\frac{m_{m_1} m_{m_2} \gamma_{\mathcal{F}_d}}{\left(m_{s_1}-1\right)\left(m_{s_2}-1\right)\bar{\gamma}_1\bar{\gamma}_2}\right) \quad (15)$$

where the PDFs of $X_{nm,i}$ and $Y_{nm,i}$ for $i = 1, N$ are, respectively,

$$p_{X_{nm,i}}(x_{nm,i}) = \frac{2\left(m_{m_i}/\Omega_{m_i}\right)^{m_{m_i}} x_{nm,i}^{2m_{m_i}-1}}{\Gamma\left(m_{m_i}\right)} e^{-\frac{m_{m_i}}{\Omega_{m_i}} x_{nm,i}^2} \tag{17}$$

$$p_{Y_{nm,i}}(y_{nm,i}) = \frac{2\left(\left(m_{s_i}-1\right)/\Omega_{s_i}\right)^{m_{s_i}} y_{nm,i}^{2m_{s_i}-1}}{\Gamma\left(m_{s_i}\right)} e^{-\frac{m_{s_i}-1}{\Omega_{s_i}} y_{nm,i}^2} \tag{18}$$

The m_{m_i} and m_{s_i} are N-FS $\mathcal{F}$ multi-path and shadowing severity parameters of i-th hop, respectively, whereas $\Omega_{m_i} = \Omega_i$ is the N-FS $\mathcal{F}$ average power of i-th hop and $\Omega_{s_i} = 1$. Similarly, the composite N-FS $\mathcal{F}$ CFM becomes equivalent to the cascaded N-Nakagami-m (for $m_{s_i} \to \infty$) and N-Rayleigh (for $m_{s_i} \to \infty$ and $m_{m_i} = 1$) fading models.

A. LEVEL CROSSING RATE

Level crossing rate (LCR) of N-FS $\mathcal{F}$ CFM for a predetermined threshold z_{th} can be obtained from the following expression [52, eq. (4)], [77]

$$N_{Z_{\mathcal{F}_N}}(z_{th}) = \int_0^\infty \dot{z}_{\mathcal{F}_N} p_{Z_{\mathcal{F}_N}\dot{Z}_{\mathcal{F}_N}}(z_{th}, \dot{z}_{\mathcal{F}_N}) d\dot{z}_{\mathcal{F}_N} \tag{19}$$

where, $p_{Z_{\mathcal{F}_N}\dot{Z}_{\mathcal{F}_N}}(z_{\mathcal{F}_N}, \dot{z}_{\mathcal{F}_N})$ is the joint distribution of $Z_{\mathcal{F}_N}$ and its first derivative $\dot{Z}_{\mathcal{F}_N}$. From (16), $X_{nm,1}$ can be expressed as

$$X_{nm,1} = \frac{Z_{\mathcal{F}_N} \prod_{i=1}^N Y_{nm,i}}{\prod_{i=2}^N X_{nm,i}} \tag{20}$$

Moreover, $p_{Z_{\mathcal{F}_N}\dot{Z}_{\mathcal{F}_N}}(z_{\mathcal{F}_N}, \dot{z}_{\mathcal{F}_N})$ can be written as $2N$-1 folded, integral-form expression of the joint PDF of i.n.i.d RVs, $Z_{\mathcal{F}_N}, \dot{Z}_{\mathcal{F}_N}, Y_{nm,1}, X_{nm,2}, Y_{nm,2}, \ldots, X_{nm,N}$ and $Y_{nm,N}$, as follows from [65, eq. (12)]. The equation is given at the bottom of the next page, where $p_{Z_{\mathcal{F}_N}\dot{Z}_{\mathcal{F}_N}Y_{nm,1}X_{nm,2}\cdots Y_{nm,N}}$ for independent RVs can be written as [65, eq. (13)]

$$\begin{aligned} &p_{Z_{\mathcal{F}_N}\dot{Z}_{\mathcal{F}_N}Y_{nm,1}X_{nm,2}\cdots Y_{nm,N}}(z_{\mathcal{F}_N}\dot{z}_{\mathcal{F}_N}y_{nm,1}x_{nm,2}\cdots y_{nm,N}) \\ &= p_{\dot{Z}_{\mathcal{F}_N}|Z_{\mathcal{F}_N}Y_{nm,1}X_{nm,2}\cdots Y_{nm,N}}(\dot{z}_{\mathcal{F}_N}|z_{\mathcal{F}_N}y_{nm,1}\cdots y_{nm,N}) \\ &\quad \times p_{Z_{\mathcal{F}_N}|Y_{nm,1}X_{nm,2}\cdots Y_{nm,N}}(z_{\mathcal{F}_N}|y_{nm,1}x_{nm,2}\cdots y_{nm,N}) \\ &\quad \times p_{Y_{nm,1}}(y_{nm,1}) p_{X_{nm,2}}(x_{nm,2}) \cdots p_{Y_{nm,N}}(y_{nm,N}) \end{aligned} \tag{22}$$

The $p_{Z_{\mathcal{F}_N}|Y_{nm,1}X_{nm,2}\cdots Y_{nm,N}}(z_{\mathcal{F}_N}|y_{nm,1}x_{nm,2}\cdots y_{nm,N})$ with a help of (20) can be expressed further as

$$\begin{aligned} &p_{Z_{\mathcal{F}_N}|Y_{nm,1}X_{nm,2}\cdots Y_{nm,N}}(z_{\mathcal{F}_N}|y_{nm,1}x_{nm,2}\cdots y_{nm,N}) \\ &= \left|\frac{dx_{nm,1}}{dz_{\mathcal{F}_N}}\right| p_{X_{nm,1}}\left(\frac{z_{\mathcal{F}_N}\prod_{i=1}^N y_{nm,i}}{\prod_{i=2}^N x_{nm,i}}\right) \end{aligned} \tag{23}$$

From ((19)-(23)), the $N_{Z_{\mathcal{F}_N}}(z_{th})$ of N-FS $\mathcal{F}$ CFM can be written as expression (24), shown at the bottom of the page.

From (16), the first derivative of $Z_{\mathcal{F}_N}$ can be expressed as

$$\begin{aligned} \dot{Z}_{\mathcal{F}_N} = \prod_{i=1}^N \frac{X_{nm,i}}{Y_{nm,i}} \Bigg(&\frac{\dot{X}_{nm,1}}{X_{nm,1}} - \frac{\dot{Y}_{nm,1}}{Y_{nm,1}} + \frac{\dot{X}_{nm,2}}{X_{nm,2}} - \frac{\dot{Y}_{nm,2}}{Y_{nm,2}} \\ &\cdots + \frac{\dot{X}_{nm,N}}{X_{nm,N}} - \frac{\dot{Y}_{nm,N}}{Y_{nm,N}} \Bigg) \end{aligned} \tag{25}$$

It is important to note that the first derivatives of $2N$ zero-mean (ZM) independent Gaussian RVs $X_{nm,1}, Y_{nm,1}, X_{nm,2}, Y_{nm,2}, \ldots, X_{nm,N}$ and $Y_{nm,N}$ denoted as, respectively $\dot{X}_{nm,1}, \dot{Y}_{nm,1}, \dot{X}_{nm,2}, \dot{Y}_{nm,2}, \ldots, \dot{X}_{nm,N}$ and $\dot{Y}_{nm,N}$ are also $2N$ ZM independent Gaussian RVs. Since the linear transformation of independent Gaussian RVs is a Gaussian RV, $p_{\dot{Z}_{\mathcal{F}_N}|Z_{\mathcal{F}_N}Y_{nm,1}\cdots Y_{nm,N}}(\dot{z}_{\mathcal{F}_N}|z_{\mathcal{F}_N}y_{nm,1}\cdots y_{nm,N})$ has a conditional Gaussian distribution with the variance $\sigma^2_{\dot{Z}_{\mathcal{F},N}}$ and mean

$$\begin{aligned} \bar{\dot{Z}}_{\mathcal{F}_N} = \prod_{i=1}^N \frac{X_{nm,i}}{Y_{nm,i}} \Bigg(&\frac{\bar{\dot{X}}_{nm,1}}{X_{nm,1}} - \frac{\bar{\dot{Y}}_{nm,1}}{Y_{nm,1}} + \frac{\bar{\dot{X}}_{nm,2}}{X_{nm,2}} - \frac{\bar{\dot{Y}}_{nm,2}}{Y_{nm,2}} \\ &\cdots + \frac{\bar{\dot{X}}_{nm,N}}{X_{nm,N}} - \frac{\bar{\dot{Y}}_{nm,N}}{Y_{nm,N}} \Bigg) = 0 \end{aligned} \tag{26}$$

where $\bar{\dot{X}}_{nm,1}, \bar{\dot{Y}}_{nm,1}, \bar{\dot{X}}_{nm,2}, \bar{\dot{Y}}_{nm,2}, \ldots, \bar{\dot{X}}_{nm,N}$ and $\bar{\dot{Y}}_{nm,N}$ are the mean values of $\dot{X}_{nm,1}, \dot{Y}_{nm,1}, \dot{X}_{nm,2}, \dot{Y}_{nm,2}, \ldots, \dot{X}_{nm,N}$ and $\dot{Y}_{nm,N}$, respectively.

Based on (25) and with some additional mathematical manipulations, the $\sigma^2_{\dot{Z}_{\mathcal{F},N}}$ can be expressed as (27), given on the next page, where the variances $\sigma^2_{\dot{X}_{nm,i}}$, $i = 1, N$ and $\sigma^2_{\dot{Y}_{nm,i}}$, $i = 1, N$ are respectively, $\sigma^2_{\dot{X}_{nm,i}} = \pi^2 f^2_{m_{x_i}}(\frac{\Omega_{m_i}}{m_{m_i}})$ and $\sigma^2_{\dot{Y}_{nm,i}} = \pi^2 f^2_{m_{y_i}}(\frac{\Omega_{s_i}}{m_{s_i}-1})$ as provided in [78, eq. (4)] and [52],

$$\begin{aligned} p_{Z_{\mathcal{F}_N}\dot{Z}_{\mathcal{F}_N}}(z_{\mathcal{F}_N}, \dot{z}_{\mathcal{F}_N}) = &\int_0^\infty dx_{nm,2} \cdots \int_0^\infty dx_{nm,N} \int_0^\infty dy_{nm,1} \int_0^\infty dy_{nm,2} \cdots \int_0^\infty dy_{nm,N} \\ &\times p_{Z_{\mathcal{F}_N}\dot{Z}_{\mathcal{F}_N}Y_{nm,1}X_{nm,2}\cdots Y_{nm,N}}(z_{\mathcal{F}_N}\dot{z}_{\mathcal{F}_N}y_{nm,1}x_{nm,2}\cdots y_{nm,N}) \end{aligned} \tag{21}$$

$$\begin{aligned} N_{Z_{\mathcal{F}_N}}(z_{th}) = &\int_0^\infty dx_{nm,2} \int_0^\infty dx_{nm,3} \cdots \int_0^\infty dx_{nm,N} \int_0^\infty dy_{nm,1} \int_0^\infty dy_{nm,2} \cdots \int_0^\infty dy_{nm,N} \\ &\times \left|\frac{dx_{nm,1}}{dz_{\mathcal{F}_N}}\right| p_{X_{nm,1}}\left(\frac{z_{th}\prod_{i=1}^N y_{nm,i}}{\prod_{i=2}^N x_{nm,i}}\right) p_{X_{nm,2}}(x_{nm,2}) \cdots p_{X_{nm,N}}(x_{nm,N}) \\ &\times p_{Y_{nm,1}}(y_{nm,1}) p_{Y_{nm,2}}(y_{nm,2}) \cdots p_{Y_{nm,N}}(y_{nm,N}) \int_0^\infty \dot{z}_{\mathcal{F}_N} p_{\dot{Z}_{\mathcal{F}_N}|Z_{\mathcal{F}_N}\cdots Y_{nm,N}}(\dot{z}_{\mathcal{F}_N}|z_{th}\cdots y_{nm,N}) d\dot{z}_{\mathcal{F}_N} \end{aligned} \tag{24}$$

respectively. Moreover, in the case of N-FS $\mathcal{F}$ CFM, $\Omega_{m_i} = \Omega_i$ and $\Omega_{s_i} = 1$. It can be assumed further that the maximum Doppler frequencies are $f_m = f_{m_{x_i}} = f_{m_{y_i}}$.

In accordance with (25)-(26), the integral expression $\int_0^\infty \dot{z}_{\mathcal{F}_N} p_{\dot{Z}_{\mathcal{F}_N}|Z_{\mathcal{F}_N}\cdots Y_{nm,N}}(\dot{z}_{\mathcal{F}_N}|z_{th}\cdots y_{nm,N}) d\dot{z}_{\mathcal{F}_N}$ in (24) for the case when $p_{\dot{Z}_{\mathcal{F}_N}|Z_{\mathcal{F}_N}\cdots Y_{nm,N}}(\dot{z}_{\mathcal{F}_N}|z_{th}\cdots y_{nm,N})$ has a conditional ZM Gaussian distribution can be evaluated as

$$\int_0^\infty \dot{z}_{\mathcal{F}_N} p_{\dot{Z}_{\mathcal{F}_N}|Z_{\mathcal{F}_N}\cdots Y_{nm,N}}\left(\dot{z}_{\mathcal{F}_N}|z_{th}\cdots y_{nm,N}\right) d\dot{z}_{\mathcal{F}_N}$$
$$= \frac{1}{\sqrt{2\pi}\sigma_{\dot{Z}_{\mathcal{F},N}}} \int_0^\infty \dot{z}_{\mathcal{F}_N} e^{-\frac{1}{2}\frac{\dot{z}^2_{\mathcal{F}_N}}{\sigma^2_{\dot{Z}_{\mathcal{F},N}}}} d\dot{z}_{\mathcal{F}_N} = \frac{\sigma_{\dot{Z}_{\mathcal{F},N}}}{\sqrt{2\pi}} \quad (28)$$

It is important to note that a similar analytical approach for derivation of (28) has been performed for the case of the s-order statistical evaluation of the Nakagami-m RV [79, eq. (16)], product of two independent Nakagami-m RVs [78, eq. (8)], the ratio of two independent Nakagami-m RVs [80, eq. (20)] and the product of N independent Rayleigh RVs [65, eq. (17)].

After introducing (17), (18) and (28) in (24), the LCR of N-FS $\mathcal{F}$ for a given threshold z_{th}, yields

$$N_{Z_{\mathcal{F}_N}}(z_{th}) = \frac{2^{2N}}{\sqrt{2\pi}} \prod_{i=1}^{N} \frac{m_{m_i}^{m_{m_i}} \left(m_{s_i}-1\right)^{m_{s_i}}}{\Omega_i^{m_{m_i}} \Gamma\left(m_{m_i}\right)\Gamma\left(m_{s_i}\right)} z_{th}^{2m_{m_1}-1} L \quad (29)$$

where, L is 2N-1 folded, I-F expression provided as (30) shown at the bottom of the page.

1) EXACT LCR FOR $N = 1$

A closed-form LCR expression of FS $\mathcal{F}$ RV can be derived from the integral-form LCR expression given by (29). From (27-30), the LCR for $N = 1$ can be written as

$$N_{Z_{\mathcal{F}}}(z_{th}) = \frac{4 m_{m_1}^{m_{m_1}} \left(m_{s_1}-1\right)^{m_{s_1}} z_{th}^{2m_{m_1}-1}}{\sqrt{2\pi}\Omega_1^{m_{m_1}} \Gamma\left(m_{m_1}\right)\Gamma\left(m_{s_1}\right)} L_1 \quad (31)$$

where L_1 is one-folded integral-form expression given by

$$L_1 = \int_0^\infty dy_{nm,1} \sqrt{\frac{1}{y_{nm,1}^2}\sigma^2_{\dot{X}_{nm,1}} \left(1 + z_{th}^2 \frac{\sigma^2_{\dot{Y}_{nm,1}}}{\sigma^2_{\dot{X}_{nm,1}}}\right)} \times y_{nm,1}^{2m_{s_1}+2m_{m_1}-1} e^{-\frac{m_{m_1}}{\Omega_1} z_{th}^2 y_{nm,1}^2 - (m_{s_1}-1) y_{nm,1}^2} \quad (32)$$

Interestingly, the LCR of the N-FS $\mathcal{F}$ CFM provided in (31), after using [76, eq. (3.381.4)] and some additional mathematical manipulations reduces for $N = 1$ to the recently published LCR expression of the composite $\mathcal{F}$ fading model [52, eq. (13)]

$$N_{Z_{\mathcal{F}}}(z_{th}) = \frac{\sqrt{2\pi} f_m \Gamma\left(m_{m_1}+m_{s_1}-1/2\right)\left(m_{m_1}\right)^{m_{m_1}-1/2}}{\Gamma\left(m_{m_1}\right)\Gamma\left(m_{s_1}\right)} \times \frac{\left(\left(m_{s_1}-1\right)\Omega_1\right)^{m_{s_1}-1/2} z_{th}^{2m_{m_1}-1}}{\left(\Omega_1\left(m_{s_1}-1\right)+m_{m_1} z_{th}^2\right)^{m_{m_1}+m_{s_1}-1}} \quad (33)$$

The LCR expression of FS $\mathcal{F}$ can be useful for s-order performance analysis between two communication nodes.

2) LCR APPROXIMATION FOR N=1

The general Laplace approximation (GLA) formula has been initially proven by authors in [81], whereas in [82] authors have shown that the GLA formula fits well with exact expressions for the cases where the real-valued parameter γ takes small values. It has also been used in practice as a reliable and fast-computing mathematical tool for evaluation of many-folded integral-form expressions [54], [63], [65], [77], [78], [83], [84], [85] such as (29). In order to provide a detailed application of the GLA for evaluation of many-folded integral-form expressions, first we provide a closed-form approximate LCR expressions for $N = 1$. Although the exact closed-form LCR expression is already provided in (33), here we present a derivation of an approximate LCR expression using the GLA formula for $N = 1$,

$$\sigma^2_{\dot{Z}_{\mathcal{F},N}} = \frac{1}{x_{nm,1}^2} \prod_{i=1}^{N} \frac{x_{nm,i}^2}{y_{nm,i}^2} \sigma^2_{\dot{X}_{nm,1}} \Bigg(1 + \frac{z^2_{\mathcal{F}_N} x^2_{nm,1}}{y^2_{nm,1}} \prod_{i=1}^{N} \frac{y^2_{nm,i}}{x^2_{nm,i}} \sigma^2_{\dot{Y}_{nm,1}}/\sigma^2_{\dot{X}_{nm,1}} + \frac{z^2_{\mathcal{F}_N} x^2_{nm,1}}{x^2_{nm,2}} \prod_{i=1}^{N} \frac{y^2_{nm,i}}{x^2_{nm,i}} \sigma^2_{\dot{X}_{nm,2}}/\sigma^2_{\dot{X}_{nm,1}}$$
$$+ \frac{z^2_{\mathcal{F}_N} x^2_{nm,1}}{y^2_{nm,2}} \prod_{i=1}^{N} \frac{y^2_{nm,i}}{x^2_{nm,i}} \sigma^2_{\dot{Y}_{nm,2}}/\sigma^2_{\dot{X}_{nm,1}} + \frac{z^2_{\mathcal{F}_N} x^2_{nm,1}}{x^2_{nm,3}} \prod_{i=1}^{N} \frac{y^2_{nm,i}}{x^2_{nm,i}} \sigma^2_{\dot{X}_{nm,3}}/\sigma^2_{\dot{X}_{nm,1}}$$
$$\cdots + \frac{z^2_{\mathcal{F}_N} x^2_{nm,1}}{y^2_{nm,N}} \prod_{i=1}^{N} \frac{y^2_{nm,i}}{x^2_{nm,i}} \sigma^2_{\dot{X}_{nm,N}}/\sigma^2_{\dot{X}_{nm,1}} + \frac{z^2_{\mathcal{F}_N} x^2_{nm,1}}{x^2_{nm,N}} \prod_{i=1}^{N} \frac{y^2_{nm,i}}{x^2_{nm,i}} \sigma^2_{\dot{Y}_{nm,N}}/\sigma^2_{\dot{X}_{nm,1}} \Bigg) \quad (27)$$

$$L = \int_0^\infty dx_{nm,2} \int_0^\infty dx_{nm,3} \cdots \int_0^\infty dx_{nm,N} \int_0^\infty dy_{nm,1} \int_0^\infty dy_{nm,2} \cdots \int_0^\infty dy_{nm,N}$$
$$\times x_{nm,2}^{2m_{m_2}-2m_{m_1}-1} x_{nm,3}^{2m_{m_3}-2m_{m_1}-1} \cdots x_{nm,N}^{2m_{m_N}-2m_{m_1}-1} y_{nm,1}^{2m_{s_1}+2m_{m_1}-1} y_{nm,2}^{2m_{s_2}+2m_{m_1}-1} \cdots y_{nm,N}^{2m_{s_N}+2m_{m_1}-1} \sigma_{\dot{Z}_{\mathcal{F},N}}$$
$$\times e^{-\frac{m_{m_1}}{\Omega_1}\frac{z_{th}^2 \prod_{i=1}^{N} y^2_{nm,i}}{\prod_{i=2}^{N} x^2_{nm,i}} - \frac{m_{m_2}}{\Omega_2} x^2_{nm,2} - \frac{m_{m_3}}{\Omega_3} x^2_{nm,3} \cdots - \frac{m_{m_N}}{\Omega_N} x^2_{nm,N} - (m_{s_1}-1) y^2_{nm,1} - (m_{s_2}-1) y^2_{nm,2} \cdots - (m_{s_N}-1) y^2_{nm,N}} \quad (30)$$

as the simplest case since the GLA formula will be further utilized for derivation of an approximate closed-form LCR expression for general N. The GLA formula for the evaluation of one-folded integral expression in (32), can be written as [78, eq. (12)]

$$\int_0^\infty f_1\left(y_{nm,1}\right)e^{-\gamma f_2\left(y_{nm,1}\right)}dy_{nm,1} \approx \left(\frac{2\pi}{\gamma}\right)^{\frac{1}{2}}\frac{f_1\left(\tilde{y}_{nm,1}\right)}{\sqrt{\frac{\partial^2 f_2\left(\tilde{y}_{nm,1}\right)}{\partial y_{nm,1}^2}}}e^{-\gamma f_2\left(\tilde{y}_{nm,1}\right)} \tag{34}$$

where $f_1(y_{nm,1})$ and $f_2(y_{nm,1})$ are one-variate functions of $y_{nm,1}$, whereas γ is a real-valued parameter. After the following transformation in (32)

$$y_{nm,1}^{2m_{s_1}+2m_{m_1}-2}e^{-\frac{m_{m_1}}{\Omega_1}z_{th}^2y_{nm,1}^2-(m_{s_1}-1)y_{nm,1}^2} = e^{-\frac{m_{m_1}}{\Omega_1}z_{th}^2y_{nm,1}^2-(m_{s_1}-1)y_{nm,1}^2+(2m_{s_1}+2m_{m_1}-2)ln(y_{nm,1})} \tag{35}$$

and without loss of generality, we can set $f_1 = 1$ and $f_2 = \frac{m_{m_1}z_{th}^2y_{nm,1}^2}{\Omega_1} + (m_{s_1}-1)y_{nm,1}^2 - (2m_{s_1}+2m_{m_1}-2)ln(y_{nm,1})$. The $\tilde{y}_{nm,1}$ in (34) is obtained as a real and positive value from $\partial f_2(y_{nm,1})/\partial y_{nm,1} = 0$ for $\tilde{y}_{nm,1} = y_{nm,1}$ as

$$\tilde{y}_{nm,1} = \sqrt{\frac{m_{m_1}+m_{s_1}-1}{\frac{z_{th}^2m_{m_1}}{\Omega_1}+m_{s_1}-1}} \tag{36}$$

Finally, the LCR approximation for $N = 1$ is given by

$$N_{Z_{\mathcal{F}}}(z_{th}) \approx \frac{4m_{m_1}^{m_{m_1}}\left(m_{s_1}-1\right)^{m_{s_1}}\sigma_{\dot{X}_{nm,1}}\left(1+z_{th}^2\frac{\sigma_{\dot{Y}_{nm,1}}^2}{\sigma_{\dot{X}_{nm,1}}^2}\right)^{\frac{1}{2}}}{\sqrt{2\pi}\Omega_1^{m_{m_1}}\Gamma\left(m_{m_1}\right)\Gamma\left(m_{s_1}\right)} \times \left(\frac{2\pi}{\gamma}\right)^{\frac{1}{2}}\frac{1}{\sqrt{\frac{\partial^2 f_2\left(\tilde{y}_{nm,1}\right)}{\partial y_{nm,1}^2}}}e^{-\gamma f_2\left(\tilde{y}_{nm,1}\right)}. \tag{37}$$

3) LCR APPROXIMATION FOR N=2

The integral-form LCR expression for $N = 2$ from (29) can be written as

$$N_{Z_{\mathcal{F}_d}}(z_{th}) = \frac{16}{\sqrt{2\pi}}\frac{m_{m_1}^{m_{m_1}}m_{m_2}^{m_{m_2}}\left(m_{s_1}-1\right)^{m_{s_1}}}{\Omega_1^{m_{m_1}}\Omega_2^{m_{m_2}}\Gamma\left(m_{m_1}\right)\Gamma\left(m_{m_2}\right)} \times \frac{\left(m_{s_2}-1\right)^{m_{s_2}}\sigma_{\dot{X}_{nm,1}}}{\Gamma\left(m_{s_1}\right)\Gamma\left(m_{s_2}\right)}z_{th}^{2m_{m_1}-1}L_2 \tag{38}$$

where L_2 is the three-folded integral-form expression given by (39) at the bottom of the page. In order to solve L_2 we can apply the GLA formula [85, eq. (47)]

$$\int_0^\infty dx_{nm,2}\int_0^\infty dy_{nm,1}\int_0^\infty f_1\left(y_{nm,1},x_{nm,2},y_{nm,2}\right) \times e^{-\gamma f_2\left(y_{nm,1},x_{nm,2},y_{nm,2}\right)}dy_{nm,2} \approx \left(\frac{2\pi}{\gamma}\right)^{\frac{3}{2}}\frac{f_1\left(\tilde{y}_{nm,1},\tilde{x}_{nm,2},\tilde{y}_{nm,2}\right)}{\sqrt{det\left(\tilde{\mathbf{h}}\right)}}e^{-\gamma f_2\left(\tilde{y}_{nm,1},\tilde{x}_{nm,2},\tilde{y}_{nm,2}\right)} \tag{40}$$

where $f_1(y_{nm,1}, x_{nm,2}, y_{nm,2})$ and $f_2(y_{nm,1}, x_{nm,2}, y_{nm,2})$ are three-variate functions of $y_{nm,1}$, $x_{nm,2}$ and $y_{nm,2}$. After a similar transformation as in (35), we can define $f_1(y_{nm,1}, x_{nm,2}, y_{nm,2})$ and $f_2(y_{nm,1}, x_{nm,2}, y_{nm,2})$ from (39), respectively as

$$f_1 = \left(1+z_{th}^2\frac{y_{nm,2}^2\sigma_{\dot{Y}_{nm,1}}^2}{x_{nm,2}^2\sigma_{\dot{X}_{nm,1}}^2}+z_{th}^2\frac{y_{nm,1}^2y_{nm,2}^2\sigma_{\dot{X}_{nm,2}}^2}{x_{nm,2}^4\sigma_{\dot{X}_{nm,1}}^2} + z_{th}^2\frac{y_{nm,1}^2\sigma_{\dot{Y}_{nm,2}}^2}{x_{nm,2}^2\sigma_{\dot{X}_{nm,1}}^2}\right)^{1/2} \tag{41}$$

$$f_2 = \frac{m_{m_1}}{\Omega_1}\frac{z_{th}^2y_{nm,1}^2y_{nm,2}^2}{x_{nm,2}^2}+\left(m_{s_1}-1\right)y_{nm,1}^2+\frac{m_{m_2}}{\Omega_2}x_{nm,2}^2 + \left(m_{s_2}-1\right)y_{nm,2}^2-\left(2m_{s_1}+2m_{m_1}-2\right)ln\left(y_{nm,1}\right) - \left(2m_{m_2}-2m_{m_1}\right)ln\left(x_{nm,2}\right)-\left(2m_{s_2}+2m_{m_1}-2\right)ln\left(y_{nm,2}\right) \tag{42}$$

The $\tilde{y}_{nm,1}$, $\tilde{x}_{nm,2}$ and $\tilde{y}_{nm,2}$ are real and positive values obtained from the following mathematical expressions:

$$\frac{\partial f_2\left(y_{nm,1},x_{nm,2},y_{nm,2}\right)}{\partial y_{nm,1}} = 0 \quad \frac{\partial f_2\left(y_{nm,1},x_{nm,2},y_{nm,2}\right)}{\partial x_{nm,2}} = 0 \quad \frac{\partial f_2\left(y_{nm,1},x_{nm,2},y_{nm,2}\right)}{\partial y_{nm,2}} = 0 \tag{43}$$

for $\tilde{y}_{nm,1} = y_{nm,1}$, $\tilde{x}_{nm,2} = x_{nm,2}$ and $\tilde{y}_{nm,2} = y_{nm,2}$, whereas the $\tilde{\mathbf{h}}$ is a Hessian 3×3 matrix obtain from $\mathbf{h}$ given by

$$\mathbf{h} = \begin{bmatrix} \frac{\partial^2 f_2}{\partial y_{nm,1}^2} & \frac{\partial^2 f_2}{\partial y_{nm,1}\partial x_{nm,2}} & \frac{\partial^2 f_2}{\partial y_{nm,1}\partial y_{nm,2}} \\ \frac{\partial^2 f_2}{\partial x_{nm,2}\partial y_{nm,1}} & \frac{\partial^2 f_2}{\partial x_{nm,2}^2} & \frac{\partial^2 f_2}{\partial x_{nm,2}\partial y_{nm,2}} \\ \frac{\partial^2 f_2}{\partial y_{nm,2}\partial y_{nm,1}} & \frac{\partial^2 f_2}{\partial y_{nm,2}\partial x_{nm,2}} & \frac{\partial^2 f_2}{\partial y_{nm,2}^2} \end{bmatrix} \tag{44}$$

$$L_2 = \int_0^\infty dy_{nm,1}\int_0^\infty dx_{nm,2}\int_0^\infty dy_{nm,2}\left(1+z_{th}^2\frac{y_{nm,2}^2\sigma_{\dot{Y}_{nm,1}}^2}{x_{nm,2}^2\sigma_{\dot{X}_{nm,1}}^2}+z_{th}^2\frac{y_{nm,1}^2y_{nm,2}^2\sigma_{\dot{X}_{nm,2}}^2}{x_{nm,2}^4\sigma_{\dot{X}_{nm,1}}^2}+z_{th}^2\frac{y_{nm,1}^2\sigma_{\dot{Y}_{nm,2}}^2}{x_{nm,2}^2\sigma_{\dot{X}_{nm,1}}^2}\right)^{1/2} \times y_{nm,1}^{2m_{s_1}+2m_{m_1}-2}x_{nm,2}^{2m_{m_2}-2m_{m_1}}y_{nm,2}^{2m_{s_2}+2m_{m_1}-2}e^{-\frac{m_{m_1}}{\Omega_1}\frac{z_{th}^2y_{nm,1}^2y_{nm,2}^2}{x_{nm,2}^2}-(m_{s_1}-1)y_{nm,1}^2-\frac{m_{m_2}}{\Omega_2}x_{nm,2}^2-(m_{s_2}-1)y_{nm,2}^2} \tag{39}$$

for $\tilde{y}_{nm,1} = y_{nm,1}$, $\tilde{x}_{nm,2} = x_{nm,2}$ and $\tilde{y}_{nm,2} = y_{nm,2}$. After substituting $f_1(\tilde{y}_{nm,1}, \tilde{x}_{nm,2}, \tilde{y}_{nm,2})$, $f_2(\tilde{y}_{nm,1}, \tilde{x}_{nm,2}, \tilde{y}_{nm,2})$ and $\tilde{\mathbf{h}}$ in (40), the L_2 is approximated as a closed-form expression.

4) LCR APPROXIMATION FOR GENERAL N

The GLA formula that can be used to evaluate the $2N$-1 I-F expression is [65, eq. (I.3)]

$$\begin{aligned}
&\int_0^\infty dx_{nm,2} \int_0^\infty dx_{nm,3} \cdots \int_0^\infty dx_{nm,N} \\
&\times \int_0^\infty dy_{nm,1} \int_0^\infty dy_{nm,2} \cdots \int_0^\infty dy_{nm,N} \\
&\times \int_0^\infty f_1\left(y_{nm,1}, x_{nm,2}, y_{nm,2}, \ldots, x_{nm,N}, y_{nm,N}\right) \\
&\times e^{-\gamma f_2\left(y_{nm,1}, x_{nm,2}, y_{nm,2}, \ldots, x_{nm,N}, y_{nm,N}\right)} dy_{nm,N} \\
&\approx \left(\frac{2\pi}{\gamma}\right)^{\frac{2N-1}{2}} \frac{f_1\left(\tilde{y}_{nm,1}, \tilde{x}_{nm,2}, \tilde{y}_{nm,2}, \ldots, \tilde{x}_{nm,N}, \tilde{y}_{nm,N}\right)}{\sqrt{det\left(\tilde{\mathbf{h}}\right)}} \\
&\times e^{-\gamma f_2\left(\tilde{y}_{nm,1}, \tilde{x}_{nm,2}, \tilde{y}_{nm,2}, \ldots, \tilde{x}_{nm,N}, \tilde{y}_{nm,N}\right)}
\end{aligned} \tag{45}$$

where $f_1(y_{nm,1}, x_{nm,2}, y_{nm,2}, \ldots, x_{nm,N}, y_{nm,N})$ and $f_2(y_{nm,1}, x_{nm,2}, y_{nm,2}, \ldots, x_{nm,N}, y_{nm,N})$ are multi-variate functions of $y_{nm,1}, x_{nm,2}, y_{nm,2}, \ldots, x_{nm,N}$ and $y_{nm,N}$, whereas γ is a real-valued parameter. The $\tilde{y}_{nm,1}, \tilde{x}_{nm,2}, \tilde{y}_{nm,2}, \ldots, \tilde{x}_{nm,N}$ and $\tilde{y}_{nm,N}$ are real and positive values obtained from the set of $2N-1$ differential equations,

$$\begin{aligned}
&\frac{\partial f_2\left(y_{nm,1}, x_{nm,2}, y_{nm,2}, \ldots, x_{nm,N}, y_{nm,N}\right)}{\partial y_{nm,1}} = 0, \\
&\frac{\partial f_2\left(y_{nm,1}, x_{nm,2}, y_{nm,2}, \ldots, x_{nm,N}, y_{nm,N}\right)}{\partial x_{nm,2}} = 0, \\
&\vdots \\
&\frac{\partial f_2\left(y_{nm,1}, x_{nm,2}, y_{nm,2}, \ldots, x_{nm,N}, y_{nm,N}\right)}{\partial y_{nm,N}} = 0
\end{aligned} \tag{46}$$

for $y_{nm,i} = \tilde{y}_{nm,i}$, $i = 1, N$ and $x_{nm,i} = \tilde{x}_{nm,i}$, $i = 2, N$. The $\tilde{\mathbf{h}}$ is a Hessian $(2N-1) \times (2N-1)$ matrix obtained from $\mathbf{h}$ in (47), provided at the bottom of the page, for $y_{nm,i} = \tilde{y}_{nm,i}$, $i = 1, N$ and $x_{nm,i} = \tilde{x}_{nm,i}$, $i = 2, N$. In order to apply the GLA formula for evaluation of the $2N-1$ folded integral-form expression L in (30), we set f_1 and f_2, respectively as (48) and (49), where (49) is shown at the bottom of the page.

$$\begin{aligned}
&f_1\left(y_{nm,1}, x_{nm,2}, y_{nm,2}, \ldots, x_{nm,N}, y_{nm,N}\right) \\
&= \Bigg(1 + \frac{z_{th}^2 x_{nm,1}^2}{y_{nm,1}^2} \prod_{i=1}^{N} \frac{y_{nm,i}^2}{x_{nm,i}^2} \sigma_{\dot{Y}_{nm,1}}^2 / \sigma_{\dot{X}_{nm,1}}^2 \\
&\quad + \frac{z_{th}^2 x_{nm,1}^2}{x_{nm,2}^2} \prod_{i=1}^{N} \frac{y_{nm,i}^2}{x_{nm,i}^2} \sigma_{\dot{X}_{nm,2}}^2 / \sigma_{\dot{X}_{nm,1}}^2 \\
&\quad + \frac{z_{th}^2 x_{nm,1}^2}{y_{nm,2}^2} \prod_{i=1}^{N} \frac{y_{nm,i}^2}{x_{nm,i}^2} \sigma_{\dot{Y}_{nm,2}}^2 / \sigma_{\dot{X}_{nm,1}}^2 \\
&\quad + \frac{z_{th}^2 x_{nm,1}^2}{x_{nm,3}^2} \prod_{i=1}^{N} \frac{y_{nm,i}^2}{x_{nm,i}^2} \sigma_{\dot{X}_{nm,3}}^2 / \sigma_{\dot{X}_{nm,1}}^2 \\
&\quad \cdots + \frac{z_{th}^2 x_{nm,1}^2}{y_{nm,N}^2} \prod_{i=1}^{N} \frac{y_{nm,i}^2}{x_{nm,i}^2} \sigma_{\dot{X}_{nm,N}}^2 / \sigma_{\dot{X}_{nm,1}}^2 \\
&\quad + \frac{z_{th}^2 x_{nm,1}^2}{x_{nm,N}^2} \prod_{i=1}^{N} \frac{y_{nm,i}^2}{x_{nm,i}^2} \sigma_{\dot{Y}_{nm,N}}^2 / \sigma_{\dot{X}_{nm,1}}^2 \Bigg)^{1/2}
\end{aligned} \tag{48}$$

From (29)-(30) and (45)-(49), a closed-form approximate LCR of N-FS $\mathcal{F}$ can be written as

$$\begin{aligned}
N_{Z_{\mathcal{F}_N}}(z_{th}) &\approx \left(\frac{2\pi}{\gamma}\right)^{\frac{2N-1}{2}} \frac{2^{2N} \pi f_m}{\sqrt{2\pi}} \left(\frac{\Omega_1}{m_{m_1}}\right)^{1/2} \\
&\times \prod_{i=1}^{N} \frac{\left(\frac{m_{m_i}}{\Omega_i}\right)^{m_{m_i}} \left(m_{s_i} - 1\right)^{m_{s_i}}}{\Gamma\left(m_{m_i}\right)\Gamma\left(m_{s_i}\right)} z_{th}^{2m_{m_1}-1} \\
&\times \frac{f_1\left(\tilde{y}_{nm,1}, \tilde{x}_{nm,2}, \tilde{y}_{nm,2}, \ldots, \tilde{x}_{nm,N}, \tilde{y}_{nm,N}\right)}{\sqrt{det\left(\tilde{h}\right)}} \\
&\times e^{-\gamma f_2\left(\tilde{y}_{nm,1}, \tilde{x}_{nm,2}, \tilde{y}_{nm,2}, \ldots, \tilde{x}_{nm,N}, \tilde{y}_{nm,N}\right)}.
\end{aligned} \tag{50}$$

$$\mathbf{h} = \begin{bmatrix}
\frac{\partial^2 f_2\left(y_{nm,1}, x_{nm,2}, \ldots, x_{nm,N}, y_{nm,N}\right)}{\partial y_{nm,1}^2} & \frac{\partial^2 f_2\left(y_{nm,1}, x_{nm,2}, \ldots, x_{nm,N}, y_{nm,N}\right)}{\partial y_{nm,1} \partial x_{nm,2}} & \cdots & \frac{\partial^2 f_2\left(y_{nm,1}, x_{nm,2}, \ldots, x_{nm,N}, y_{nm,N}\right)}{\partial y_{nm,1} \partial y_{nm,N}} \\
\frac{\partial^2 f_2\left(y_{nm,1}, x_{nm,2}, \ldots, x_{nm,N}, y_{nm,N}\right)}{\partial x_{nm,2} \partial y_{nm,1}} & \frac{\partial^2 f_2\left(y_{nm,1}, x_{nm,2}, \ldots, x_{nm,N}, y_{nm,N}\right)}{\partial x_{nm,2}^2} & \cdots & \frac{\partial^2 f_2\left(y_{nm,1}, x_{nm,2}, \ldots, x_{nm,N}, y_{nm,N}\right)}{\partial x_{nm,2} \partial y_{nm,N}} \\
\vdots & \vdots & & \vdots \\
\frac{\partial^2 f_2\left(y_{nm,1}, x_{nm,2}, \ldots, x_{nm,N}, y_{nm,N}\right)}{\partial y_{nm,N} \partial y_{nm,1}} & \frac{\partial^2 f_2\left(y_{nm,1}, x_{nm,2}, \ldots, x_{nm,N}, y_{nm,N}\right)}{\partial y_{nm,N} \partial x_{nm,2}} & \cdots & \frac{\partial^2 f_2\left(y_{nm,1}, x_{nm,2}, \ldots, x_{nm,N}, y_{nm,N}\right)}{\partial y_{nm,N}^2}
\end{bmatrix} \tag{47}$$

$$\begin{aligned}
f_2\left(y_{nm,1}, x_{nm,2}, y_{nm,2}, \ldots, x_{nm,N}, y_{nm,N}\right) &= \frac{m_{m_1}}{\Omega_1} \frac{z_{th}^2}{\prod_{i=1}^{N} y_{nm,i}^2 \prod_{i=2}^{N} x_{nm,i}^2} + \frac{m_{m_2}}{\Omega_2} x_{nm,2}^2 + \frac{m_{m_3}}{\Omega_3} x_{nm,3}^2 \cdots + \frac{m_{m_N}}{\Omega_N} x_{nm,N}^2 \\
&+ \left(m_{s_1} - 1\right) y_{nm,1}^2 + \left(m_{s_2} - 1\right) y_{nm,2}^2 \cdots + \left(m_{s_N} - 1\right) y_{nm,N}^2 - \left(2m_{s_1} + 2m_{m_1} - 2\right) \ln\left(y_{nm,1}\right) - \left(2m_{m_2} - 2m_{m_1}\right) \ln\left(x_{nm,2}\right) \\
&- \left(2m_{s_2} + 2m_{m_1} - 2\right) \ln\left(y_{nm,2}\right) \cdots - \left(2m_{m_N} - 2m_{m_1}\right) \ln\left(x_{nm,N}\right) - \left(2m_{s_N} + 2m_{m_1} - 2\right) \ln\left(y_{nm,N}\right)
\end{aligned} \tag{49}$$

B. AVERAGE FADE DURATION

The average fade duration (AFD) is the faded signal's average time below a threshold z_{th} and for N-FS $\mathcal{F}$ CFM it can be calculated as

$$A_{Z_{\mathcal{F}_N}}(z_{th}) = \frac{F_{Z_{\mathcal{F}_N}}(z_{th})}{N_{Z_{\mathcal{F}_N}}(z_{th})} \tag{51}$$

where $F_{Z_{\mathcal{F}_N}}$ is the CDF of N-FS $\mathcal{F}$ RP. Fortunately, the CDF of N-FS $\mathcal{F}$ RP in terms of the Meijer's G function has been recently provided in [35, eq. (13)] and is given by (52) shown at the bottom of the page. The approximate closed-form expression for AFD of N-FS $\mathcal{F}$ CFM with respect to (50)-(52) is written as (53), shown at the bottom of the page.

C. BURST ERROR RATE

Deep fades can degrade the system performances of a wireless link. During a deep fade, the faded signal envelope is below a predetermined threshold, $z_{\mathcal{F}_D} < z_{th}$ which causes symbol errors. The evaluation of the burst error rate can be useful for interleaver design of error correction codes that are usually applied as a preventive mechanism against the deep fades. The burst error rate is a process of correlated errors that are not like the f-order statistical analysis of uniformly spreading errors along time as addressed in [11] and [35] for FS $\mathcal{F}$ and N-FS $\mathcal{F}$ CFMs, respectively. Moreover, the 5G and 6G systems add the ultra-reliable low-latency communication (URLLC) which demand the performance analysis with respect to time. Indeed, the burst error rate analysis over time-varying fading channels represents useful performance metrics for various 5G and beyond 5G communication scenarios [86], [87], [88]. The burst error rate analysis based on s-order statistics of dual-hop and multi-hop relay communications over cascaded Nakagami-m and Log-normal fading channels has been considered in [61] and [66].

In this paper, the burst error rate analysis of the composite N-FS $\mathcal{F}$ distribution is addressed through time dependent s-order statistical measures $N_{Z_{\mathcal{F}_N}}(z_{th})$ and $A_{Z_{\mathcal{F}_N}}(z_{th})$ as a function of z_{th}. The burst error rate is likely to occur when a time of fade duration $A_{Z_{\mathcal{F}_N}}(z_{th})$ increases. Moreover, the burst error rate has a similar behaviour to the outage probability $F_{Z_{\mathcal{F}_N}}(z_{th})$ since the burst error rate is expected to increase for higher z_{th} values. In addition to the burst error rate analysis carried out in terms of number of hops and multi-path severities, provided in [61], [66], this paper provides the burst error rate analysis over N-FS $\mathcal{F}$ fading channels addressed in terms of shadowing severities. We evaluate the burst error rate of N-FS $\mathcal{F}$ CFM as [66, eq. (32)]

$$BE_N(z_{th}) = \frac{L_{Z_{\mathcal{F}_N}}(z_{th})\left\lceil N_{Z_{\mathcal{F}_N}}(z_{th})\right\rceil}{D_s} \tag{54}$$

The average number of lost symbols $L_{Z_{\mathcal{F}_N}}(z_{th})$ are determined as the ratio of the $A_{Z_{\mathcal{F}_N}}(z_{th})$ at a given threshold z_{th} to the symbol transmission time as

$$L_{Z_{\mathcal{F}_N}}(z_{th}) = \left\lceil \frac{A_{Z_{\mathcal{F}_N}}(z_{th})}{1/D_s} \right\rceil = \left\lceil D_s A_{Z_{\mathcal{F}_N}}(z_{th}) \right\rceil \tag{55}$$

where $D_s = 1/T_s$ is average transmission rate given in symbols/sec, T_s is transmission time per symbol and $\lceil\cdot\rceil$ is the ceiling function [89, eq. (04.02.02.0001.01)]. As observed further in [66, eq. (32)] and [61, eq. (45)], the burst error rate in (54) can't exceed unity

$$BE_N(z_{th}) = min\left\{1, \frac{L_{Z_{\mathcal{F}_N}}(z_{th})\left\lceil N_{Z_{\mathcal{F}_N}}(z_{th})\right\rceil}{D_s}\right\} \tag{56}$$

Based on (54)-(56) it can be concluded that the burst error rate presents an upper bound of the outage probability of N-FS $\mathcal{F}$ distribution for a given threshold z_{th} that can be expressed as

$$P_{Z_{\mathcal{F}_N}}(z_{th}) = P_{Z_{\mathcal{F}_N}}\left(z_{\mathcal{F}_N} \le z_{th}\right) = A_{Z_{\mathcal{F}_N}}(z_{th}) N_{Z_{\mathcal{F}_N}}(z_{th}) \tag{57}$$

Moreover, the outage probability of N-FS $\mathcal{F}$ CFM is $P_{Z_{\mathcal{F}_N}}(z_{th}) = F_{Z_{\mathcal{F}_N}}(z_{th})$, where $F_{Z_{\mathcal{F}_N}}(z_{th})$ is the CDF of N-FS $\mathcal{F}$ RV, already provided in (52). Since the minimum value of $L_{Z_{\mathcal{F}_N}}(z_{th})$ in (55) is unity, than the minimum average number of lost symbols can be given as $D_s \le \frac{1}{A_{Z_{\mathcal{F}_N}}(z_{th})}$ [61], [66, eq. (34)]. The maximum symbol rate of N-FS $\mathcal{F}$ CFM, which provides that one symbol on average is sent within each fade duration, can be determined by

$$D_s = \frac{1}{A_{Z_{\mathcal{F}_N}}(z_{th})} \tag{58}$$

$$F_{Z_{\mathcal{F}_N}}\left(z_{\mathcal{F}_N}\right) = \frac{1}{\prod_{i=1}^{N}\Gamma\left(m_i\right)\Gamma\left(m_{s_i}\right)} G_{N+1,N+1}^{N,N+1}\left(z_{\mathcal{F}_N}^2 \prod_{i=1}^{N}\frac{m_{m_i}}{\Omega_i m_{s_i}}\middle| \begin{matrix} 1-m_{s_1}, 1-m_{s_2}, \ldots, 1-m_{s_N}, 1 \\ m_{m_1}, m_{m_2}, \ldots, m_{m_N}, 0 \end{matrix}\right) \tag{52}$$

$$A_{Z_{\mathcal{F}_N}}(z_{th}) \approx \frac{\sqrt{2\pi}\left(\frac{m_{m_1}}{\Omega_1}\right)^{1/2}\prod_{i=1}^{N}\Omega_i^{m_{m,i}} G_{N+1,N+1}^{N,N+1}\left(z_{th}^2\prod_{i=1}^{N}\frac{m_{m_i}}{\Omega_i m_{s_i}}\middle| \begin{matrix} 1-m_{s_1}, 1-m_{s_2}, \ldots, 1-m_{s_N}, 1 \\ m_{m_1}, m_{m_2}, \ldots, m_{m_N}, 0 \end{matrix}\right)\sqrt{det\left(\tilde{\mathbf{h}}\right)}}{2^{2N} f_m \pi \left(\frac{2\pi}{\gamma}\right)^{\frac{2N-1}{2}}\prod_{i=1}^{N} m_{m_i}^{m_{m_i}} m_{s_i}^{m_{s_i}} z_{th}^{2m_{m_1}-1} f_1\left(\tilde{y}_{nm,1}, \tilde{x}_{nm,2}, \ldots, \tilde{y}_{nm,N}\right) e^{-\gamma f_2\left(\tilde{y}_{nm,1}, \tilde{x}_{nm,2}, \ldots, \tilde{y}_{nm,N}\right)}} \tag{53}$$

FIGURE 1. Block scheme of multi-hop relaying system.

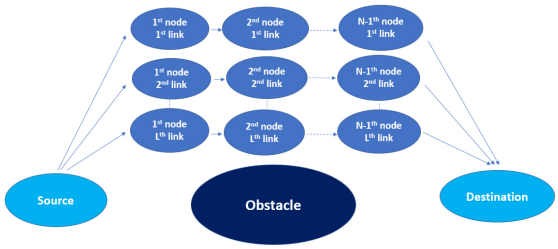

FIGURE 2. Cooperative multi-hop communications in NLOS conditions.

V. PERFORMANCE OF MULTI-HOP AND COOPERATIVE MULTI-HOP COMMUNICATIONS

A. MULTI-HOP AF-RA COMMUNICATION SYSTEM

The simplified scheme of the considered N-hop AF relaying system is presented on Fig. 1. The total fading gain of N-hop communication link assisted by fixed-gain (FG) AF relays over FS $\mathcal{F}$ channels can be modeled with the N-FS $\mathcal{F}$ CFM, as previously observed for N-hop AF-RA system over Rayleigh [65, eq. (39)] and Nakagami-m [61, eq. (4)] channels. We observed the case when the gain of each relay is constant and equal to one [90]. Thus, the total fading gain can be given by $G = \prod_{i=1}^{N} Z_{\mathcal{F}_i}$. The derived statistical results for $N_{Z_{\mathcal{F}_N}}(z_{th})$, $A_{Z_{\mathcal{F}_N}}(z_{th})$, $BE_N(z_{th})$ and D_s are directly applied for performance assessment of N-hop FG AF-relaying system over FS $\mathcal{F}$ channels and numerically evaluated in the next section.

B. COOPERATIVE MULTI-HOP AF-RA COMMUNICATION SYSTEM IN NLOS CONDITIONS

Cooperative N-hop communications in N-LOS propagation conditions assisted by L parallel independent links with S-S at reception is presented in Fig. 2. The signal envelope at the output of the considered cooperative system can be given by $Z_{\mathcal{F}_L} = max(Z_{\mathcal{F}_N}{}^{(1)}, \ldots, Z_{\mathcal{F}_N}{}^{(j)}, \ldots, Z_{\mathcal{F}_N}{}^{(L)})$ [63, eq. (7)], where $Z_{\mathcal{F}_N}{}^{(j)}$ is the signal envelope of j-th parallel link modeled with N-FS $\mathcal{F}$ distribution. The CDF at the output of cooperative system established through L independent N-hop AF-RA links with S-S at reception is [63, eqs. (8–9)]

$$F_{Z_{\mathcal{F}_L}}(z_{\mathcal{F}_L}) = \left(F_{z_{\mathcal{F}_N}}(z_{\mathcal{F}_L})\right)^L \tag{59}$$

where $F_{Z_{\mathcal{F}_N}}$ is the CDF of N-FS $\mathcal{F}$ CFM provided in (52). The LCR at the output of the observed cooperative system for the threshold z_{th} can be given by [63, eq. (23)]

$$N_{Z_{\mathcal{F}_L}}(z_{th}) = L \times N_{Z_{\mathcal{F}_N}}(z_{th}) F_{Z_{\mathcal{F}_N}}(z_{th})^{L-1} \tag{60}$$

where the $N_{Z_{\mathcal{F}_N}}(z_{th})$ is provided in (29). The AFD is obtained from the previously derived expressions as

$$A_{Z_{\mathcal{F}_L}}(z_{th}) = \frac{F_{Z_{\mathcal{F}_L}}(z_{th})}{N_{Z_{\mathcal{F}_L}}(z_{th})} \tag{61}$$

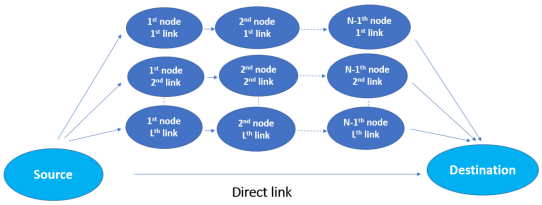

FIGURE 3. Cooperative multi-hop communications in LOS conditions.

Based on (54)-(56), the burst error rate for the considered case can be written as

$$BE_L(z_{th}) = min\left\{1, \frac{\left\lceil D_s A_{Z_{\mathcal{F}_L}}(z_{th})\right\rceil \left\lceil N_{Z_{\mathcal{F}_L}}(z_{th})\right\rceil}{D_s}\right\} \tag{62}$$

The provided s-order statistics for $N_{Z_{\mathcal{F}_L}}(z_{th})$, $A_{Z_{\mathcal{F}_L}}(z_{th})$ and $BE_L(z_{th})$ are directly applied to the cooperative communications in N-LOS propagation conditions and numerically presented in the numerical and simulation results.

C. COOPERATIVE MULTI-HOP COMMUNICATIONS IN LOS CONDITIONS

The cooperative communications in LOS propagation conditions established through independent direct link and L independent N-hop RA links over FS $\mathcal{F}$ channels with S-S at reception is presented in Fig. 3. Similarly, the signal envelope at the output can be written as $Z_{\mathcal{F}_{D,L}} = max(Z_{\mathcal{F}}, Z_{\mathcal{F}_N}{}^{(1)}, \ldots Z_{\mathcal{F}_N}{}^{(j)}, \ldots Z_{\mathcal{F}_N}{}^{(L)})$, where $Z_{\mathcal{F}}$ is the signal envelope given by (1). The CDF of the cooperative scenario in the presence of the LOS conditions can be written as

$$F_{Z_{\mathcal{F}_{D,L}}}(z_{\mathcal{F}_{D,L}}) = \left(F_{z_{\mathcal{F}_N}}(z_{\mathcal{F}_{D,L}})\right)^L F_{z_{\mathcal{F}}}(z_{\mathcal{F}_{D,L}}) \tag{63}$$

where $F_{z_{\mathcal{F}}}$ is provided in (6). The LCR of the cooperative system under LOS conditions with S-S at reception over FS $\mathcal{F}$ fading channels is [63, eq. (22)]

$$N_{Z_{\mathcal{F},D,L}}(z_{th}) = N_{Z_{\mathcal{F},L}}(z_{th}) F_{z_{\mathcal{F}}}(z_{th}) + N_{z_{\mathcal{F}}}(z_{th}) F_{Z_{\mathcal{F},D,L}}(z_{th}) \tag{64}$$

where $N_{z_{\mathcal{F}}}$ is provided in (33). The AFD of the considered cooperative system in LOS conditions can be given by

$$A_{Z_{\mathcal{F},D,L}}(z_{th}) = \frac{F_{Z_{\mathcal{F},D,L}}(z_{th})}{N_{Z_{\mathcal{F},D,L}}(z_{th})} \tag{65}$$

Finally, the burst error rate for the considered case is

$$BE_{D,L}(z_{th}) = min\left\{1, \frac{\left\lceil D_s A_{Z_{\mathcal{F}_{D,L}}}(z_{th})\right\rceil \left\lceil N_{Z_{\mathcal{F}_{D,L}}}(z_{th})\right\rceil}{D_s}\right\} \tag{66}$$

The $N_{Z_{\mathcal{F}_{D,L}}}(z_{th})$, $A_{Z_{\mathcal{F}_{D,L}}}(z_{th})$ and $BE_{D,L}(z_{th})$ are directly used for performance analysis of the cooperative communications in LOS propagation conditions and graphically presented in the following section.

TABLE 2. Simulation parameters.

Parameter	Notation	Value
Average powers	Ω_i	1
Carrier frequency	f_c	1 GHz
Envelope threshold	z_{th}	0 dB, 3 dB
Maximum Doppler frequencies	$f_m = f_{m_s} = f_{m_d}$	74.0741 Hz
Multi-path severities	m_{m_i}	1-4
Number of hops	N	1-4
Number of parallel multi-hop links	L	1-3
Relative velocities	$v = v_s = v_d$	80 km/h
Shadowing severities	m_{s_i}	1-4
Speed of the light	c	3×10^8 m/s
Transmission symbol rate	D_s	10^5 symbols/s

VI. NUMERICAL AND SIMULATION RESULTS

In this section we provide the numerically evaluated integral-form and approximate closed-form results for multi-hop FG AF-RA communications in terms of $N_{Z_{\mathcal{F}_N}}(z_{th})$, $A_{Z_{\mathcal{F}_N}}(z_{th})$, $BE_N(z_{th})$ and D_s. Moreover, this section provides the numerical results for cooperative multi-hop AF relay communications assisted by L parallel links in NLOS conditions for $N_{Z_{\mathcal{F}_L}}(z_{th})$, $A_{Z_{\mathcal{F}_L}}(z_{th})$, $BE_L(z_{th})$ a well as multi-hop AF relay communications in LOS conditions for $N_{Z_{\mathcal{F}_{D,L}}}(z_{th})$, $A_{Z_{\mathcal{F}_{D,L}}}(z_{th})$, $BE_{D,L}(z_{th})$. The considered theoretical results for the observed N-FS $\mathcal{F}$ CFM system parameters are compared with M-C simulations, where the simulation parameters are summarized in Table 2. We simulate a cooperative multi-hop FG AF-relaying system for different number of hops and different values of N-FS $\mathcal{F}$ CFM severity parameters. The carrier frequency used for the simulation is $f_c = 1$ GHz while the source and destination relative velocities are taken to be the same $v = v_s = v_d = 80$km/h. The maximum Doppler frequencies of the source (f_{ms}) and destination (f_{md}) nodes are calculated as $f_m = f_{ms} = f_{md} = vf_{c/c}$, where $c = 3 \times 10^8$ m/s. Moreover, similar simulation parameters are used in [66].

A. LCR AND AFD OF MULTI-HOP COMMUNICATIONS OVER N-FS $\mathcal{F}$ CHANNELS

Numerical results for s-order statistical measures in terms of AFD and LCR of N-FS $\mathcal{F}$ distribution and their application to multi-hop AF-RA communications for identically and non-identically distributed fading parameters obtained from exact integral-form and approximate closed-form mathematical expressions are presented in Figs. 4–8. It can be noticed that the approximate expressions fit well with the exact expressions for the $\gamma = 1$ and observed system values. Although the complexity of the GLA formula for obtaining the LCR approximations increases for higher N, it can be efficiently implemented for the considered N with the help of standardized software tools such as MATLAB or MATHEMATICA. Moreover, the presented s-order results are confirmed by M-C simulations.

Fig. 4. shows the normalized LCR for different values of N, multi-path and shadowing severities of N-FS $\mathcal{F}$ CFM. As expected, more severe multi-path and shadowing fading conditions (e.g., when all $m_{m_i} = m_{s_i} = 2$) cause $N_{Z_{\mathcal{F}_N}}(z_{th})/f_m$ to take higher values in the low threshold area.

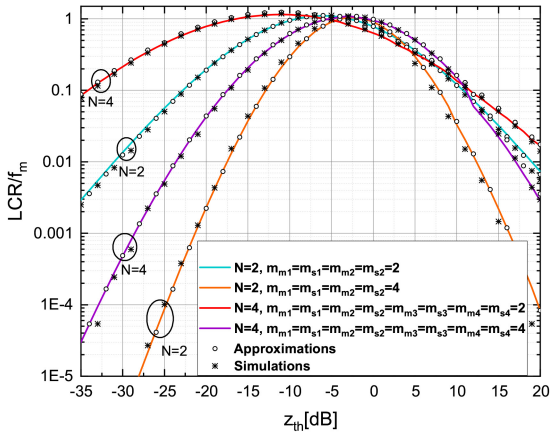

FIGURE 4. Normalized LCR of N-Fisher-Snedecor $\mathcal{F}$ CFM observed for various N and various values of identically distributed fading parameters.

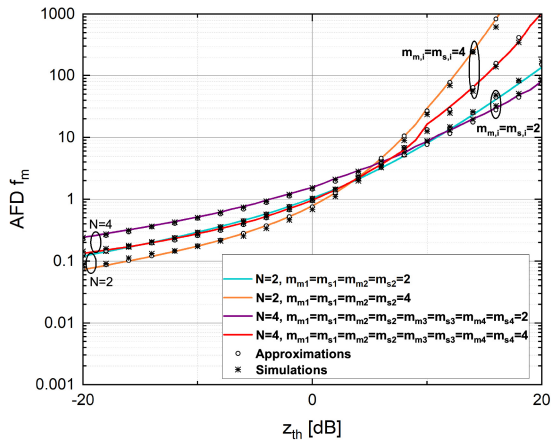

FIGURE 5. Normalized AFD of N-Fisher-Snedecor $\mathcal{F}$ CFM observed for various N and various values of identically distributed fading parameters.

A change of multi-path and shadowing severity conditions (e.g., shift from $m_{m_i} = m_{s_i} = 2$ to $m_{m_i} = m_{s_i} = 4$) causes a decrease of $N_{Z_{\mathcal{F}_N}}(z_{th})/f_m$ for low z_{th} values. Contrary, the increase in the number of hops (N) causes the normalised $N_{Z_{\mathcal{F}_N}}(z_{th})$ to increase in the low threshold area. The values of $A_{Z_{\mathcal{F}_N}}(z_{th})$ multiplied by f_m for the various system values of cascaded N-FS $\mathcal{F}$ CFM in the case of identically distributed fading parameters are presented in Fig. 5. It can be seen that by increasing the value of N, $A_{Z_{\mathcal{F}_N}}(z_{th})f_m$ increases for lower threshold values while it decreases for higher threshold values. It can be further observed that by increasing N-FS $\mathcal{F}$ CFM multi-path and shadowing severity parameters, $A_{Z_{\mathcal{F}_N}}(z_{th})f_m$ decreases for lower threshold values. Moreover, the impact of N on $A_{Z_{\mathcal{F}_N}}(z_{th})f_m$ for lower z_{th} is stronger than N-FS $\mathcal{F}$ CFM multi-path and shadowing severities, while the impact of severities is more dominant for higher z_{th}. It can be concluded that s-order system performance improvement for lower thresholds can be achieved for lower values of N (e.g., when $N = 1$) and higher values of multi-path and shadowing severities.

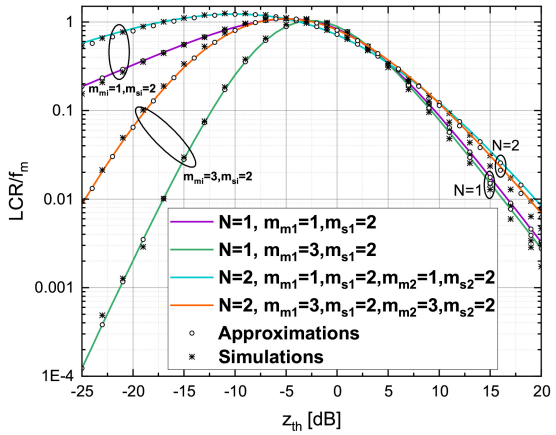

FIGURE 6. Normalized LCR of N-Fisher-Snedecor $\mathcal{F}$ CFM observed for various N and various identically and non-identically distributed fading parameters.

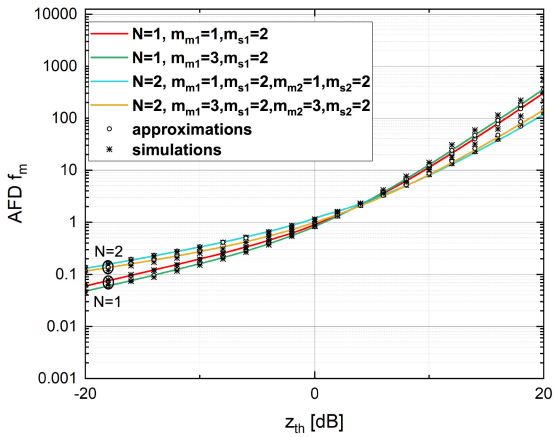

FIGURE 7. Normalized AFD of N-Fisher-Snedecor $\mathcal{F}$ CFM observed for various N and various identically and non-identically distributed fading parameters.

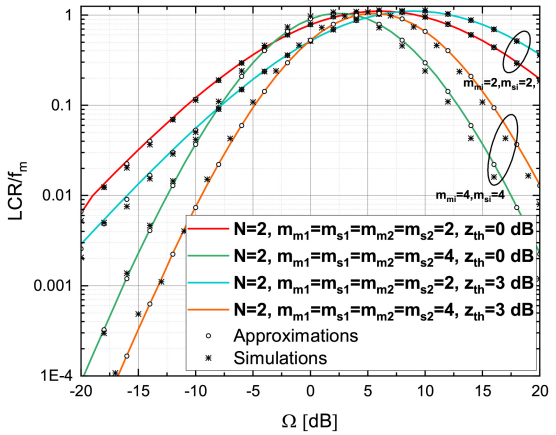

FIGURE 8. Normalized LCR of N-Fisher-Snedecor $\mathcal{F}$ CFM versus Ω observed for $N = 2$, various z_{th} values and various N-FS $\mathcal{F}$ CFM fading parameters.

Fig. 6 shows $N_{Z_{\mathcal{F}_N}}(z_{th})/f_m$ for different values of N, multi-path and shadowing severities. Moreover, Fig. 6 includes the cases of non-identically distributed fading parameters of N-FS $\mathcal{F}$ CFM. It can be observed that $N_{Z_{\mathcal{F}_N}}(z_{th})/f_m$ increases in the region of lower threshold when multi-path fading conditions shift from less severe to severe (e.g., shift from $m_{m_1} = 1$ to $m_{m_1} = 3$). As observed previously for identically distributed FS $\mathcal{F}$ fading channels, an increase in N (e.g., change from $N = 2$ to $N = 1$) causes $N_{Z_{\mathcal{F}_N}}(z_{th})/f_m$ to decrease, especially for lower z_{th}. It can be noticed that $N_{Z_{\mathcal{F}_N}}(z_{th})/f_m$ for $N = 1$ and $m_{m_1} = 1$, $m_{s_1} = 2$ as well as for $N = 1$ and $m_{m_1} = 3$, $m_{s_1} = 2$ coincides with the LCR for the same set of multi-path and shadowing severities provided in [52], as expected. The exact and approximate $A_{Z_{\mathcal{F}_N}}(z_{th})f_m$ expressions for different values of N, multi-path and shadowing severities with non-identically distributed fading parameters of FS $\mathcal{F}$ CFM are presented in Fig. 7. One can notice that $A_{Z_{\mathcal{F}_N}}(z_{th})f_m$ decreases in the region of lower threshold for lower values of N while a decrease in multi-path fading conditions from less severe to severe (e.g., shift from $m_{m_1} = 3$ to $m_{m_1} = 1$) causes a slight increase in $A_{Z_{\mathcal{F}_N}}(z_{th})f_m$ for lower thresholds. The values of $A_{Z_{\mathcal{F}_N}}(z_{th})f_m$ for the special case of ($N = 1$, $m_{m_1} = 1$, $m_{s_1} = 2$) and ($N = 1$, $m_{m_1} = 3$, $m_{s_1} = 2$) has the same behavior as the AFD, already reported in [52]. Fig. 8 presents the normalized $N_{Z_{\mathcal{F}_N}}$ as a function of Ω ($\Omega = \Omega_1 = \Omega_2$) for $N = 2$ and for different N-FS $\mathcal{F}$ CFM multi-path and shadowing severity conditions. The normalised $N_{Z_{\mathcal{F}_N}}$ takes small values in boundary regions. It can be expected that for the small values of Ω, $z_{\mathcal{F}_N} < z_{th}$, while for the higher values of Ω, $z_{\mathcal{F}_N} > z_{th}$. It can be noticed that the normalized $N_{Z_{\mathcal{F}_N}}$ in a high average power region is influenced by N-FS $\mathcal{F}$ CFM multi-path and shadowing severity conditions. Namely, less severe fading conditions (e.g., when $m_{m_1} = m_{m_2} = m_{s_1} = m_{s_2} = 4$) provide less number of crossings if compared with more severe fading conditions (e.g., when $m_{m_1} = m_{m_2} = m_{s_1} = m_{s_2} = 4$). As expected, the lower z_{th} values decrease the normalized $N_{Z_{\mathcal{F}_N}}$.

B. BURST ERROR RATE AND MAXIMUM SYMBOL RATE OF MULTI-HOP COMMUNICATIONS OVER N-FS $\mathcal{F}$ CHANNELS

The numerical results for the burst error rate and maximum data rate of N-FS $\mathcal{F}$ distribution for various sets of system model parameters evaluated from exact integral-form and approximate closed-form expressions are compared with M-C simulations on Figures 9–11, respectively. The burst error rate is evaluated for constant $f_m = 74.0741$ Hz and $D_s = 10^5$ symbols/s and for different N-FS $\mathcal{F}$ CFM parameters. It can be observed on Fig. 9. that the system performance improvement in relation to the burst error rate can be achieved by decreasing the number of hops and by increasing the values of multi-path and fading severity parameters of N-FS $\mathcal{F}$ CFM, since the burst error rate decreases. A similar observation for the burst error rate behaviour in relation to multi-path severity parameters has been noticed in [66] while the decrease of the burst error rate with increase of number of hops has been noticed in [61]. Fig. 10 shows the burst error rate as a function of Ω for $N = 2$ and for different N-FS $\mathcal{F}$ CFM system model parameters. It is

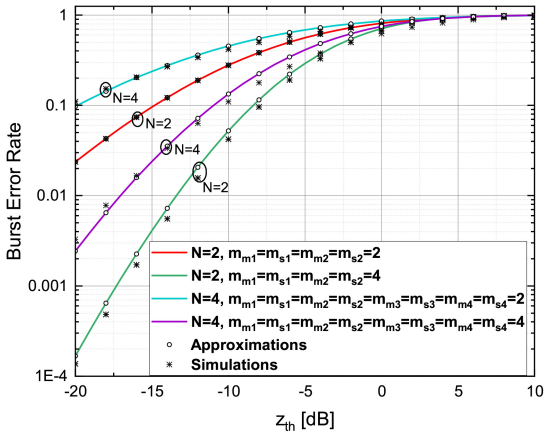

FIGURE 9. Burst Error Rate of N-Fisher-Snedecor $\mathcal{F}$ CFM for various N, various fading severities and constant $f_m = 74.0741$ Hz and $D_S = 10^5$ symbols/s.

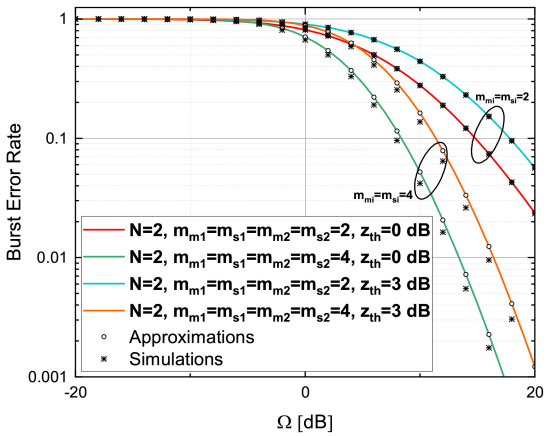

FIGURE 10. Burst Error Rate of N-Fisher-Snedecor $\mathcal{F}$ CFM versus Ω for $N = 2$, various z_{th} values, various fading severities and constant $f_m = 74.0741$ Hz and $D_S = 10^5$ symbols/s.

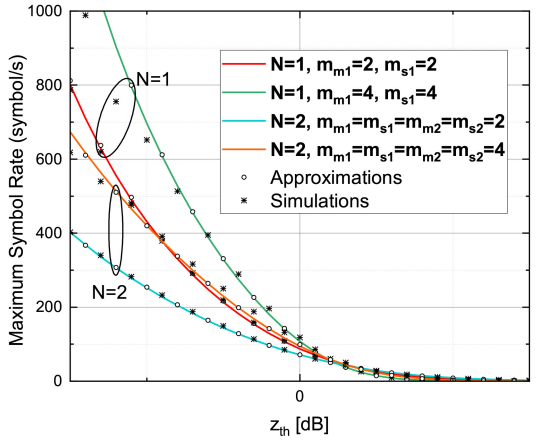

FIGURE 11. Maximum Symbol Rate of N-Fisher-Snedecor $\mathcal{F}$ CFM observed for various N, various fading severities values and constant $f_m = 74.0741$ Hz.

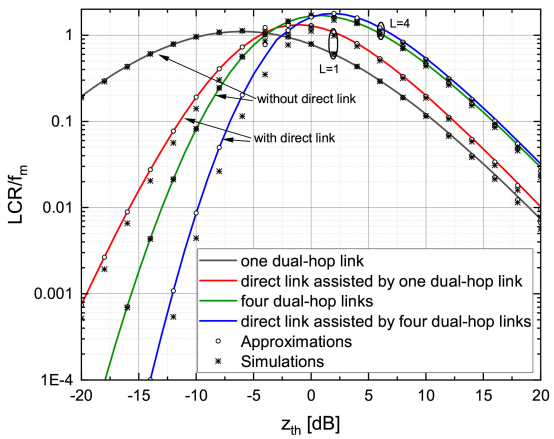

FIGURE 12. Normalized LCR for cooperative multi-hop scenario observed for $N = 2$ and different link settings.

obvious that the high average power region is influenced by N-FS $\mathcal{F}$ CFM severity conditions. The system performance improvement in relation to BE_N in high average power region can be achieved in less severe composite fading conditions, as expected. The lower z_{th} values cause decrease in the BE_N. The maximum symbol rate over N-FS $\mathcal{F}$ CFM for a set of different system model parameters and constant $f_m = 74.0741$ Hz is observed in Fig. 11. The maximum symbol rate is evaluated as $D_s = 1/A_{Z_{\mathcal{F}_N}}(z_{th})$. The maximum D_s is limited by the threshold value and is dependant on N-FS $\mathcal{F}$ CFM fading severity parameters and number of hops. As expected, the maximum D_s increases with a decrease in the number of hops and increase in fading severity values.

C. S-ORDER STATISTICS AND BURST ERROR RATE OF COOPERATIVE MULTI-HOP COMMUNICATIONS OVER N-FS $\mathcal{F}$ CHANNELS

The $N_{Z_{\mathcal{F},L}}$ versus z_{th} for $N = 2$, N-FS $\mathcal{F}$ CFM severities ($m_{m_1} = 2$, $m_{s_1} = 2$, $m_{m_2} = 2$, $m_{s_2} = 2$), average powers ($\Omega_1 = \Omega_2 = 1$) and different L as well as $N_{Z_{\mathcal{F},D,L}}$ versus z_{th} for $N = 2$, N-FS $\mathcal{F}$ CFM severities ($m_{m_1} = 2$, $m_{s_1} = 2$, $m_{m_2} = 2$, $m_{s_2} = 2$), FS $\mathcal{F}$ CFM severities ($m_m = 2$ and $m_s = 2$), average powers ($\Omega = \Omega_1 = \Omega_2 = 1$) and different L are presented on Fig. 12. As expected, the $N_{Z_{\mathcal{F},D,L}}(z_{th})$ provides lower normalized LCR values for lower thresholds than $N_{Z_{\mathcal{F},L}}(z_{th})$. Moreover, the impact of the absence of direct LOS link on the LCR of cooperative AF-RA multi-hop communications with S-S at reception is stronger for lower z_{th} dB values and for lower number of redundant (parallel) dual-hop AF-RA links. The BE_L and $BE_{D,L}$ versus z_{th} for $N = 2$, N-FS $\mathcal{F}$ severities ($m_{m,1} = 2$, $m_{s,1} = 2$, $m_{m,2} = 2$, $m_{s,2} = 2$), FS $\mathcal{F}$ severities ($m = 2$ and $m_s = 2$), average powers ($\Omega = \Omega_1 = \Omega_2 = 1$) and different L are presented on Fig. 13. The burst error rate for the observed system model configuration can be decreased by increasing the number of available dual-hop parallel links. Moreover, the absence of direct LOS link on the burst error rate can be compensated by adding one or more dual-hop redundant links (e.g., $BE_{D,L}$ of a cooperative system with direct link assisted by one dual-hop AF-RA link has a similar behavior

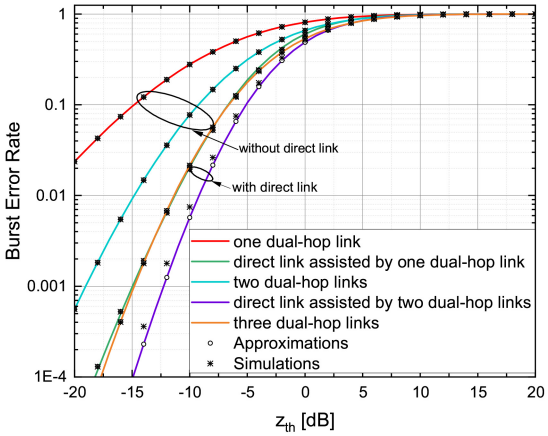

FIGURE 13. Burst Error Rate for cooperative multi-hop scenario observed for $N = 2$, constant $f_m = 74.0741$ Hz, $D_S = 10^5$ symbols/s and different link settings.

as BE_L of a cooperative system established through three parallel dual-hop AF-RA links).

The s-order statistics and burst error rate of the observed dual-hop and cooperative dual-hop AF-RA communications (when $N = 2$) are derived and numerically evaluated by using novel analytical expressions of double FS $\mathcal{F}$ CFM (e.g., the CDF of double FS $\mathcal{F}$ CFM provided in (14) has been directly used for the derivation and numerical evaluation of the AFD expressions provided in (51), (61) and (65) as well as for the burst error rate expressions provided in (56), (62) and (66) for the special case when $N = 2$).

Although the derived s-order statistical results are developed for isotropic scattering conditions, as previously observed for different mobile and vehicular systems in [49], [61], [62], [63], [64], [65], [66], they can be useful for s-order and burst error rate performance analysis of cooperative multi-hop AF-RA V2X systems over composite fading channels in LOS, N-LOS and N-LOSv communication conditions.

VII. CONCLUSION

This paper provides accurate closed-form approximations for LCR and AFD of N-FS $\mathcal{F}$ distribution. The novel and fast-computing s-order statistical closed-form approximate results fit well with the exact integral-form results and M-C simulations. The mathematical proof that the LCR formula of N-FS $\mathcal{F}$ distribution for $N = 1$ reduces to the recently published results of composite $\mathcal{F}$ fading model has been provided. Capitalizing on the derived s-order statistical expressions, analytical and numerical results for the bust error rate and maximum data rate of N-FS $\mathcal{F}$ CFM are provided and applied to the multi-hop and cooperative multi-hop AF-RA communications established trough independent direct and L parallel links with S-S at destination. In general, the system performance improvement of the AF-RA multi-hop communication system in the lower threshold regime can be achieved by shifting from severe to less severe multi-path and shadowing fading conditions and by decreasing the number of hops, since AFD and burst error rate decrease. Numerical results for AF-RA multi-hop communications point out that the maximum symbol rate can be increased for lower thresholds in less severe multi-path and shadowing fading conditions and for small number of hops. The cooperative AF-RA multi-hop communication performance improvement in terms of the burst error rate can be achieved by adding more redundant (parallel) multi-hop links. Moreover, the impact of the absence of direct LOS link on the burst error rate can be decreased by adding more redundant links. The provided s-order statistical results for cooperative multi-hop AF-RA communications assisted by L parallel links with and without direct LOS link over FS $\mathcal{F}$ CFM with S-S at destination can be useful for designing V2X systems in LOS, N-LOS and N-LOSv communication conditions.

REFERENCES

[1] C.-X. Wang, J. Bian, J. Sun, W. Zhang, and M. Zhang, "A survey of 5G channel measurements and models," *IEEE Commun. Surveys Tuts.*, vol. 20, no. 4, pp. 3142–3168, 4th Quart., 2018.

[2] H. Suzuki, "A statistical model for urban radio propagation," *IEEE Trans. Commun.*, vol. 25, no. 7, pp. 673–680, Jul. 1977.

[3] F. Hansen and F. I. Meno, "Mobile fading—Rayleigh and log-normal superimposed," *IEEE Trans. Veh. Technol.*, vol. 26, no. 4, pp. 332–335, Nov. 1977.

[4] P. M. Shankar, "Error rates in generalized shadowed fading channels," *Wireless Personal Commun.*, vol. 28, no. 3, pp. 233–238, 2004.

[5] I. M. Kostić, "Analytical approach to performance analysis for channel subject to shadowing and fading," *IEE Proc. Commun.*, vol. 156, no. 6, pp. 821–827, 2005.

[6] A. Abdi and M. Kaveh, "K distribution: An appropriate substitute for Rayleigh-lognormal distribution in fading-shadowing wireless channels," *Electron. Lett.*, vol. 34, no. 9, pp. 851–852, 1998.

[7] P. S. Bithas, N. C. Sagias, P. T. Mathiopoulos, G. K. Karagiannidis, and A. A. Rontogiannis, "On the performance analysis of digital communications over generalized-K fading channels," *IEEE Commun. Lett.*, vol. 10, no. 5, pp. 353–355, May 2006.

[8] H. Al-Hmood and H. S. Al-Raweshidy, "Unified modeling of composite $\kappa-\mu$/Gamma, $\eta-\mu$/Gamma, and $\alpha-\mu$/Gamma fading channels using a mixture gamma distribution with applications to energy detection," *IEEE Antennas Wireless Propag. Lett.*, vol. 16, pp. 104–108, 2016.

[9] S. K. Yoo et al., "The κ-μ/inverse gamma and η-μ/inverse gamma composite fading models: Fundamental statistics and empirical validation," *IEEE Trans. Commun.*, vol. 69, no. 8, pp. 5514–5530, Aug. 2021, doi: 10.1109/TCOMM.2017.2780110.

[10] N. Simmons, C. R. N. D. Silva, S. L. Cotton, P. C. Sofotasios, S. K. Yoo, and M. D. Yacoub, "On shadowing the κ-μ fading model," *IEEE Access*, vol. 8, pp. 120513–120536, 2020.

[11] S. K. Yoo, S. L. Cotton, P. C. Sofotasios, M. Matthaiou, M. Valkama, and G. K. Karagiannidis, "The Fisher–Snedecor $\mathcal{F}$ distribution: A simple and accurate composite fading model," *IEEE Commun. Lett.*, vol. 21, no. 7, pp. 1661–1664, Jul. 2017.

[12] M. K. Simon and M. S. Alouini, *Digital Communication Over Fading Channels*. Hoboken, NJ, USA: Wiley, 2005.

[13] J. Zhang, H. Du, Q. Sun, B. Ai, and D. W. K. Ng, "Physical layer security enhancement with reconfigurable intelligent surface-aided networks," *IEEE Trans. Inf. Forensics Security*, vol. 16, pp. 3480–3495, 2021.

[14] K. O. Odeyemi, P. A. Owolawi, and O. O. Olakanmi, "Reconfigurable intelligent surface assisted mobile network with randomly moving user over Fisher-Snedecor fading channel," *Phys. Commun.*, vol. 43, Dec. 2020, Art. no. 101186.

[15] A. Makarfi, K. Rabie, O. Kaiwartya, O. Badarneh, G. Nauryzbayev, and R. Kharel, "Physical layer security in RIS-assisted networks in fisher-snedecor composite fading," in *Proc. 12th Int. Symp. Commun. Syst., Netw. Digit. Signal Process. (CSNDSP)*, 2020, pp. 1–6.

[16] A. U. Makarfi, K. M. Rabie, O. Kaiwartya, O. S. Badarneh, X. Li, and R. Kharel, "Reconfigurable intelligent surface enabled IoT networks in generalized fading channels," in *Proc. IEEE Int. Conf. Commun. (ICC)*, 2020, pp. 1–6.

[17] F. R. Ghadi and W. P. Zhu, "RIS-aided secure communications over Fisher-Snedecor F fading channels," Aug. 2022, *arXiv:2208.07274*.

[18] A. U. Makarfi et al., "Performance analysis of SWIPT networks over composite fading channels," in *Proc. IEEE 8th Int. Conf. Commun. Netw. (ComNet)*, 2020, pp. 1–7.

[19] H. Al-Hmood and H. S. Al-Raweshidy, "Selection combining scheme over non-identically distributed Fisher-Snedecor $\mathcal{F}$ fading channels," *IEEE Wireless Commun. Lett.*, vol. 10, no. 4, pp. 840–843, Apr. 2021, doi: 10.1109/LWC.2020.3046519.

[20] W. Cheng, X. Wang, T. Ma, and G. Wang, "On the performance analysis of switched diversity combining receivers over Fisher–Snedecor $\mathcal{F}$ composite fading channels," *Sensors*, vol. 21, no. 9, p. 3014, 2021.

[21] O. S. Badarneh, D. B. da Costa, P. C. Sofotasios, S. Muhaidat, and S. L. Cotton, "On the sum of Fisher–Snedecor $\mathcal{F}$ variates and its application to maximal-ratio combining," *IEEE Wireless Commun. Lett.*, vol. 7, no. 6, pp. 966–969, Dec. 2018.

[22] H. Du, J. Zhang, J. Cheng, and B. Ai, "Sum of Fisher-Snedecor F random variables and its applications,," *IEEE Open J. Commun. Soc.*, vol. 1, pp. 342–356, 2020.

[23] P. Zhang, J. Zhang, K. P. Peppas, D. W. K. Ng, and B. Ai, "Dual-hop relaying communications over Fisher-Snedecor $\mathcal{F}$-fading channels," *IEEE Trans. Commun.*, vol. 68, no. 5, pp. 2695–2710, May 2020.

[24] S. K. Yoo et al., "A comprehensive analysis of the achievable channel capacity in $\mathcal{F}$ composite fading channels," *IEEE Access*, vol. 7, pp. 34078–34094, 2019.

[25] H. Zhao, L. Yang, A. S. Salem, and M.-S. Alouini, "Ergodic capacity under power adaption over Fisher–Snedecor $\mathcal{F}$ fading channels," *IEEE Commun. Lett.*, vol. 23, no. 3, pp. 546–549, Mar. 2019.

[26] H. Zhao, "Power adaption over fluctuating two-ray fading channels and Fisher-Snedecor F fading channels," Ph.D. dissertation, Dept. Comput. Electr. Math. Sci. Eng. Division, King Abdullah Univ. Sci. Technol., Thuwal, Saudi Arabia, 2019.

[27] F. S. Almehmadi and O. S. Badarneh, "On the effective capacity of Fisher–Snedecor $\mathcal{F}$ fading channels," *Electron. Lett.*, vol. 54, no. 18, pp. 1068–1070, 2018.

[28] S. Chen, J. Zhang, G. K. Karagiannidis, and B. Ai, "Effective rate of MISO systems over Fisher–Snedecor $\mathcal{F}$ fading channels," *IEEE Commun. Lett.*, vol. 22, no. 12, pp. 2619–2622, Dec. 2018.

[29] P. C. Sofotasios et al., "Effective rate over F composite fading channels," in *Proc. IEEE Wireless Commun. Netw. Conf. (WCNC)*, 2019, pp. 1–6, doi: 10.1109/WCNC.2019.8886144.

[30] P. C. Sofotasios and S. K. Yoo, "Achievable fixed rate capacity in emerging wireless systems (invited paper)," in *Proc. Int. Conf. Adv. Commun. Technol. Netw. (CommNet)*, 2019, pp. 1–9, doi: 10.1109/COMMNET.2019.8742381.

[31] L. Kong and G. Kaddoum, "On physical layer security over the Fisher-Snedecor $\mathcal{F}$ wiretap fading channels," *IEEE Access*, vol. 6, pp. 39466–39472, 2018.

[32] O. S. Badarneh, P. C. Sofotasios, S. Muhaidat, S. L. Cotton, K. M. Rabie, and N. Aldhahir, "Achievable physical-layer security over composite fading channels," *IEEE Access*, vol. 8, pp. 195772–195787, 2020.

[33] F. Rostami Ghadi and W.-P. Zhu, "Performance analysis over correlated/independent Fisher-Snedecor $\mathcal{F}$ fading multiple access channels," *IEEE Trans. Veh. Technol.*, vol. 71, no. 7, pp. 7561–7571, Jul. 2022, doi: 10.1109/TVT.2022.3169568.

[34] S. K. Yoo, P. C. Sofotasios, S. L. Cotton, S. Muhaidat, O. S. Badarneh, and G. K. Karagiannidis, "Entropy and energy detection-based spectrum sensing over $\mathcal{F}$-composite fading channels," *IEEE Trans. Commun.*, vol. 67, no. 7, pp. 4641–4653, Jul. 2019.

[35] O. S. Badarneh, S. Muhaidat, P. C. Sofotasios, S. L. Cotton, K. Rabie, and D. B. da Costa, "The N*Fisher-Snedecor $\mathcal{F}$ cascaded fading model," in *Proc. 14th Int. Conf. Wireless Mobile Comput. Netw. Commun. (WiMob)*, 2018, pp. 1–7.

[36] O. S. Badarneh, P. C. Sofotasios, S. Muhaidat, S. L. Cotton, and D. B. Da Costa, "Product and ratio of product of Fisher-Snedecor $\mathcal{F}$ variates and their applications to performance evaluations of wireless communication systems," *IEEE Access*, vol. 8, pp. 215267–215286, 2020.

[37] H. Du, J. Zhang, K. P. Peppas, H. Zhao, B. Ai, and X. Zhang, "On the distribution of the ratio of products of Fisher-Snedecor $\mathcal{F}$ random variables and its applications," *IEEE Trans. Veh. Technol.*, vol. 69, no. 2, pp. 1855–1866, Feb. 2020.

[38] F. Yilmaz and M. S. Alouini, "Product of the powers of generalized Nakagami-m variates and performance of cascaded fading channels," in *Proc. IEEE Global Telecommun. Conf.*, 2009, pp. 1–8.

[39] I. Trigui, A. Laourine, S. Affes, and A. Stephenne, "On the performance of cascaded generalized K fading channels," in *Proc. IEEE Global Telecommun. Conf.*, 2009, pp. 1–5.

[40] N. Bhargav, C. R. N. da Silva, Y. J. Chun, É. J. Leonardo, S. L. Cotton, and M. D. Yacoub, "On the product of two κ–μ random variables and its application to double and composite fading channels," *IEEE Trans. Wireless Commun.*, vol. 17, no. 4, pp. 2457–2470, Apr. 2019.

[41] A. R. Ndjiongue, T. M. N. Ngatched, O. A. Dobre, A. G. Armada, and H. Haas, "Analysis of RIS-based terrestrial-FSO link over GG turbulence with distance and jitter ratios," *J. Lightw. Technol.*, vol. 39, no. 21, pp. 6746–6758, Nov. 1, 2021.

[42] A. Bekkali, S. Zou, A. Kadri, M. Crisp, and R. V. Penty, "Performance analysis of passive UHF RFID systems under cascaded fading channels and interference effects," *IEEE Trans. Wireless Commun.*, vol. 14, no. 3, pp. 1421–1433, Mar. 2014.

[43] P. S. Bithas, V. Nikolaidis, A. G. Kanatas, and G. K. Karagiannidis, "UAV-to-ground communications: Channel modeling and UAV selection," *IEEE Trans. Commun.*, vol. 68, no. 8, pp. 5135–5144, Aug. 2020.

[44] E. J. Leonardo, D. B. da Costa, U. S. Dias, and M. D. Yacoub, "The ratio of independent arbitrary α-μ random variables and its application in the capacity analysis of spectrum sharing systems," *IEEE Commun. Lett.*, vol. 16, no. 11, pp. 1776–1779, Nov. 2012.

[45] C. R. N. Da Silva, N. Simmons, E. J. Leonardo, S. L. Cotton, and M. D. Yacoub, "Ratio of two envelopes taken from α-μ, η-μ, and κ-μ variates and some practical applications," *IEEE Access*, vol. 7, pp. 54449–54463, 2019.

[46] A. Matović, E. Mekić, N. Sekulović, M. Stefanović, M. Matović, and C. Stefanović, "The distribution of the ratio of the products of two independent-variates and its application in the performance analysis of relaying communication systems," *Math. Problems Eng.*, vol. 2013, Mar. 2013, Art. no. 147106.

[47] L. G. Stuber, *Principles of Mobile Communication*. Norwell, MA, USA: Kluwer Acad., 1996.

[48] H. D. Le and A. T. Pham, "Level crossing rate and average fade duration of satellite-to-UAV FSO channels," *IEEE Photon. J.*, vol. 13, no. 1, pp. 1–14, Feb. 2021.

[49] P. S. Bithas, A. G. Kanatas, D. B. da Costa, P. K. Upadhyay, and U. S. Dias, "On the double-generalized gamma statistics and their application to the performance analysis of V2V communications," *IEEE Trans. Commun.*, vol. 66, no. 1, pp. 448–460, Jan. 2018.

[50] Q. Zhu, N. Cheng, X. Chen, W. Zhong, B. Hua, and Y. Wang, "Envelope level crossing rate and average fade duration of a generic 3D non-stationary UAV channel model," *IEEE Access*, vol. 8, pp. 143134–143143, 2020.

[51] C. A. Gutirrez, M. Pätzold, N. M. Ortega, C. A. Azurdia-Meza, and F. M. Maciel-Barboza, "Doppler shift characterization of wideband mobile radio channels," *IEEE Trans. Veh. Technol.*, vol. 68, no. 12, pp. 12375–12380, Dec. 2019.

[52] S. K. Yoo, S. L. Cotton, P. C. Sofotasios, S. Muhaidat, and G. K. Karagiannidis, "Level crossing rate and average fade duration in F composite fading channels," *IEEE Wireless Commun. Lett.*, vol. 9, no. 3, pp. 281–284, Mar. 2020.

[53] W. Cheng and X. Wang, "Bivariate Fisher–Snedecor F distribution and its applications in wireless communication systems," *IEEE Access*, vol. 8, pp. 146342–146360, 2020.

[54] C. Stefanovic, M. Morales-Céspedes, R. Róka, and A. G. Armada, "Performance analysis of N-Fisher-Snedecor $\mathcal{F}$ fading and its application to N-hop FSO communications," in *Proc. 17th IEEE Int. Symp. Wireless Commun. Syst. (ISWCS)*, Berlin, Germany, Sep. 2021, pp. 1–6.

[55] C. Stefanovic, M. M. Céspedes, and A. G. Armada "Performance analysis of RIS-assisted FSO communications over Fisher–Snedecor F turbulence channels," *Appl. Sci.*, vol. 11, no. 21, 2021, Art. no. 10149.

[56] R. A. Pedriali, E. J. Leonardo, and M. D. Yacoub, "Higher order statistics for composite fading models," *IEEE Wireless Commun. Lett.*, vol. 8, no. 5, pp. 1493–1497, Oct. 2019.

[57] L. Yang, M. O. Hasna, and M.-S. Alouini,, "Average outage duration of multihop communication systems with regenerative relays," *IEEE Trans. Wireless Commun.*, vol. 4, no. 4, pp. 1366–1371, Jul. 2005.

[58] J. Tian, Q. Zhang, and S. H. Ting, "LCR and AFD of decode-and-forward relay networks with N-th best relay selection schemes in Rayleigh fading channels," *IEEE Wireless Commun. Lett.*, vol. 1, no. 4, pp. 380–383, Aug. 2012.

[59] Y. A. Chau and K. Y. T. Huang, "On the second-order statistics of correlated cascaded Rayleigh fading channels," *Int. J. Antennas Propag.*, vol. 2012, Jul. 2012, Art. no. 108534. [Online]. Available: https://doi.org/10.1155/2012/108534

[60] G. Rafiq, B. O. Hogstad, and M. Pätzold, "On the first-and second-order statistics of the capacity of N* Nakagami-m channels for applications in cooperative networks," *EURASIP J. Wireless Commun. Netw.*, vol. 2012, no. 1, pp. 1–13, 2012.

[61] F. J. Lopez-Martinez, E. Kurniawan, R. Islam, and A. Goldsmith, "Average fade duration for amplify-and-forward relay networks in fading channels," *IEEE Trans. Wireless Commun.*, vol. 14, no. 10, pp. 5454–5467, Oct. 2015.

[62] R. N. de Souza, E. E. B. Olivo, L. C. de Freitas Ferreira, C. R. N. da Silva, and J. C. S. S. Filho, "High-SNR second-order statistics of amplify-and-forward relaying with variable gains and multiple hops," in *Proc. XXXVIII Simpósio Brasileiro Telecomunicações Processamento Sinais*, 2020, pp. 1–5.

[63] N. Hajri, R. Khedhiri, and N. Youssef, "On selection combining diversity in dual-hop relaying systems over double Rice channels: Fade statistics and performance analysis," *IEEE Access*, vol. 8, pp. 72188–72203, 2020.

[64] B. Talha and M. Päetzold, "Channel models for mobile-to-mobile cooperative communication systems: A state of the art review," *IEEE Veh. Technol. Mag.*, vol. 6, no. 2, pp. 33–43, Jun. 2011.

[65] Z. Hadzi-Velkov, N. Zlatanov, and G. K. Karagiannidis, "On the second order statistics of the multihop Rayleigh fading channel," *IEEE Trans. Commun.*, vol. 57, no. 6, pp. 1815–1823, Jun. 2009.

[66] Y. A. Chau and K. Y.-T. Huang, "Burst-error analysis of dual-hop fading channels based on the second-order channel statistics," *IEEE Trans. Veh. Technol.*, vol. 59, no. 6, pp. 3108–3115, Jul. 2010.

[67] M. H. C. Garcia et al., "A tutorial on 5G NR V2X communications," *IEEE Commun. Surveys Tuts.*, vol. 23, no. 3, pp. 1972–2026, 3rd Quart., 2021.

[68] B. C. Nguyen, T. M. Hoang, and L. T. Dung, "Performance analysis of vehicle-to-vehicle communication with full-duplex amplify-and-forward relay over double-Rayleigh fading channels," *Veh. Commun.*, vol. 19, Oct. 2019, Art. no. 100166.

[69] B. E. Y. Belmekki, A. Hamza, and B. Escrig, "On the outage probability of cooperative 5G NOMA at intersections," in *Proc. IEEE 89th Veh. Technol. Conf. (VTC-Spring)*, 2019, pp. 1–6.

[70] C. Tunc and S. S. Panwar, "Mitigating the impact of blockages in millimeter-wave vehicular networks through vehicular relays," *IEEE Open J. Intell. Transp. Syst.*, vol. 2, pp. 225–239, 2021.

[71] Y. M. Khattabi, S. A. Alkhawaldeh, M. M. Matalgah, O. S. Badarneh, and R. Mesleh, "Vehicle-to-roadside-unit-to-vehicle communication system under different amplify-and-forward relaying schemes," *Veh. Commun.*, vol. 38, Dec. 2022, Art. no. 100539.

[72] N. Jaiswal and N. Purohit, "Performance analysis of NOMA-enabled vehicular communication systems with transmit antenna selection over double nakagami-m fading," *IEEE Trans. Veh. Technol.*, vol. 70, no. 12, pp. 12725–12741, Dec. 2021.

[73] Z. Li, L. Xiang, X. Ge, G. Mao, and H.-C. Chao, "Latency and reliability of mmWave multi-hop V2V communications under relay selections," *IEEE Trans. Veh. Technol.*, vol. 69, no. 9, pp. 9807–9821, Sep. 2020.

[74] P. S. Bithas, A. G. Kanatas, and D. W. Matolak, "Shadowing-based antenna selection for V2V communications," in *Proc. IEEE 29th Annu. Int. Symp. Personal, Indoor Mobile Radio Commun. (PIMRC)*, 2018, pp. 106–110, doi: 10.1109/PIMRC.2018.8581007.

[75] S. K. Yoo et al., "Evaluation of a switched combining based distributed antenna system (DAS) for pedestrian-to-vehicle communications," *IEEE Trans. Veh. Technol.*, vol. 70, no. 10, pp. 11005–11010, Oct. 2021.

[76] I. S. Gradshteyn and I. M. Ryzhik, *Table of Integrals, Series, and Products*. New York, NY, USA: Academic, 2000.

[77] C. Stefanovic et al., *A Framework for Statistical Channel Modeling in 5G Wireless Communication Systems*. Boca Raton, FL, USA: CRC Press, 2020, pp. 31–54.

[78] N. Zlatanov, Z. Hadzi-Velkov, and G. K. Karagiannidis, "Level crossing rate and average fade duration of the double Nakagami-m random process and application in MIMO keyhole fading channels," *IEEE Commun. Lett.*, vol. 12, no. 11, pp. 822–824, Nov. 2008.

[79] M. D. Yacoub, J. E. V. Bautista, and L. G. de Rezende Guedes, "On higher order statistics of the Nakagami-m distribution," *IEEE Trans. Veh. Technol.*, vol. 48, no. 3, pp. 790–794, May 1999.

[80] Z. Hadzi-Velkov, "Level crossing rate and average fade duration of dual selection combining with cochannel interference and Nakagami fading," *IEEE Trans. Wireless Commun.*, vol. 6, no. 11, pp. 3870–3876, Nov. 2007.

[81] L. C. Hsu, "A theorem on the asymptotic behavior of a multiple integral," *Duke Math. J.*, vol. 15, no. 3, pp. 623–632, 1948.

[82] R. Butler and A. T. A. Wood, "Laplace approximations for hypergeometric functions of matrix argument," *Ann. Stat.*, vol. 30, no. 4, pp. 1155–1177, 2001.

[83] C. Stefanovic, M. Pratesi, and F. Santucci, "Second order statistics of mixed RF-FSO relay systems and its application to vehicular networks," in *Proc. IEEE Int. Conf. Commun.*, Shanghai, China, May 2019, pp. 1–6.

[84] N. Milosevic, M. Stefanovic, Z. Nikolic, P. Spalevic, and C. Stefanovic, "Performance analysis of interference-limited mobile-to-mobile $\kappa-\mu$ fading channel," *Wireless Personal Commun.*, vol. 101, no. 3, pp. 1685–1701, 2018.

[85] C. Stefanovic, S. Panic, V. Bhatia, and N. Kumar, "On second-order statistics of the composite channel models for UAV-to-ground communications with UAV selection," *IEEE Open J. Commun. Soc.*, vol. 2, pp. 534–544, 2021.

[86] J. Demel, C. Bockelmann, and A. Dekorsy, "Burst error analysis of scheduling algorithms for 5G NR URLLC periodic deterministic communication," in *Proc. IEEE 91st Veh. Technol. Conf. (VTC-Spring)*, 2020, pp. 1–6.

[87] T. Wang, Z. Zheng, Y. Lin, S. Yao, and X. Xie, "Reliable and robust unmanned aerial vehicle wireless video transmission," *IEEE Trans. Rel.*, vol. 68, no. 3, pp. 1050–1060, Sep. 2019.

[88] F. H. El-Fouly, R. A. Ramadan, F. E. Abd El-Samie, M. Kachout, A. J. Alzahrani, and J. S. Alshudukhi, "Burst channel error reduction based on interleaving for efficient high-speed wireless communication," *Appl. Sci.*, vol. 12, no. 7, p. 3500, 2022.

[89] "The Wolfram functions site." 2020. [Online]. Available: http://functions.wolfram.com

[90] B. Talha, S. Primak, and M. Pätzold, "On the statistical properties of equal gain combining over mobile-to-mobile fading channels in cooperative networks," in *Proc. IEEE Int. Conf. Commun.*, 2010, pp. 1–6.

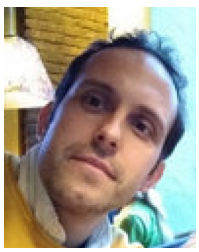

CASLAV M. STEFANOVIC (Member, IEEE) was born in Niš, Serbia, in 1982. He graduated from the Faculty of Electronic Engineering, University of Niš, Serbia. He received the M.Sc. degree in telecommunications and the Ph.D. degree from the University of Niš in 2017. Under the EUROWEB Project, he has spent ten months as a Postdoctoral Researcher with L'Aquila University, Italy. He was working as an Assistant Professor with the Faculty of Sciences and Mathematics, University of Priština, Kosovska Mitrovica, Serbia. He is the Principal Investigator on the Project within the CONEX-Plus Talent Training Program and Marie Sklodowska-Curie Actions with the Department of Signal Theory and Communications, Universidad Carlos III de Madrid, Spain. As a part of the CONEX-Plus Program, he is currently a Visiting Researcher with i2CAT, Barcelona. He has published his research results in eminent journals and conference proceedings. Some of the publications have been awarded among the best papers. His research interests include performance evaluation and channel modeling of advanced wireless communication systems.

ANA GARCÍA ARMADA (Senior Member, IEEE) received the Ph.D. degree in electrical engineering from the Polytechnical University of Madrid in February 1998. She is currently a Professor with the University Carlos III of Madrid, Spain, where she has occupied a variety of management positions (the Head of Signal Theory and Communications Department, the Vice-Dean of Electrical Engineering, a Deputy Vice-Chancellor of International Relations, among others). She is leading the Communications Research Group with the University Carlos III of Madrid. She has been a Visiting Scholar with Stanford University, Bell Labs, and University of Southampton. She has participated (and coordinated most of them) in more than 30 national and 10 international research projects as well as 20 contracts with the industry, all of them related to wireless communications. She is the coauthor of eight book chapters on *Wireless Communications and Signal Processing*. She has published more than 150 papers in international journals and conference proceedings and holds four patents. She has contributed to International Standards Organizations, such as ITU and ETSI, is a member of the Expert Group of the European 5G PPP and a member of the Advisory Committee 5JAC of the ESA as expert appointed by Spain on 5G. Her main interests are multi-carrier and multi-antenna techniques and signal processing applied to wireless communications. She has received the Young Researchers Excellence Award from the University Carlos III of Madrid. She was awarded the third place Bell Labs Prize 2014 for shaping the future of Information and Communications Technology. She received the Outstanding Service Award from the IEEE ComSoc Signal Processing and Communications Electronics Technical Committee in 2019, and the IEEE ComSoc Women in Communications Engineering Standing Committee in 2020. She has served on the editorial boards of *Physical Communication* from 2008 to 2017, *IET Communications* from 2014 to 2017, and IEEE COMMUNICATIONS LETTERS (Exemplary Editor Award 2017 and 2018). She serves on the editorial board of IEEE TRANSACTIONS ON COMMUNICATIONS and IEEE OPEN JOURNAL OF THE COMMUNICATIONS SOCIETY. She has served on the TPC of more than 40 conferences, and she has been/is part of the Organizing Committee of IEEE Globecom (2019, 2021 General Chair), IEEE Vehicular Technology Conference Fall 2018, Spring 2018 and 2019, and IEEE 5G Summit 2017, among others. She was the Newsletter Editor of the IEEE ComSoc Signal Processing and Consumer Electronics Committee from 2017 to 2018 and has been the Secretary of this committee since 2019. She has been the Secretary of the IEEE ComSoc Women in Communications Engineering Standing Committee from 2016 to 2017, and the Chair of this committee from 2018 to 2019.

XAVIER COSTA-PÉREZ (Senior Member, IEEE) received the M.Sc. and Ph.D. degrees in telecommunications from the Polytechnic University of Catalonia, Barcelona. He is a Research Professor with ICREA, the Scientific Director with i2Cat R&D Center, and the Head of Beyond 5G Networks Research and Development with NEC Laboratories Europe. His team generates research results which are regularly published at top scientific venues, produces innovations which have received several awards for successful technology transfers, participates in major European Commission Research and Development collaborative projects and contributes to standardization bodies, such as 3GPP, ETSI NFV, ETSI MEC, and IETF. His research focuses on the digital transformation of society driven by the interplay of mobile networks and AI. He was the recipient of a National Award for his Ph.D. thesis. He served on the Program Committee of several conferences (including IEEE Greencom, WCNC, and INFOCOM), published paper of high impact and holds over 50 granted patents. He served as an Editor of IEEE TRANSACTIONS ON MOBILE COMPUTING and IEEE TRANSACTIONS ON COMMUNICATIONS. He has been a 5GPPP Technology Board member.